Stability-Constrained Design for Low Voltage DC Microgrids

by

Kathleen Alison Cavanagh

B.S.E. Mechanical and Aerospace Engineering
Princeton University (2014)

Submitted to the Department of Mechanical Engineering
in partial fulfillment of the requirements for the degree of

Master of Science in Mechanical Engineering

at the

MASSACHUSETTS INSTITUTE OF TECHNOLOGY

September 2018

Author ..... Signature redacted .....
Department of Mechanical Engineering
August 17, 2018

Certified by ..... Signature redacted .....
Konstantin Turitsyn
Associate Professor, Department of Mechanical Engineering
Thesis Supervisor

Accepted by ..... Signature redacted
Rohan Abeyaratne
Chairman, Department Committee on Graduate Students
Department of Mechanical Engineering

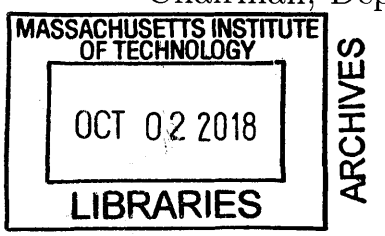

Stability-Constrained Design for Low Voltage DC Microgrids

by

Kathleen Alison Cavanagh

Submitted to the Department of Mechanical Engineering
on August 17, 2018, in partial fulfillment of the
requirements for the degree of
Master of Science in Mechanical Engineering

Abstract

Microgrids are a promising solution to reducing the energy access gap. However, microgrids are inherently fragile systems as they are not globally stable. This thesis considers two voltage instabilities that can arise in DC microgrids as a result of tightly controlled loads in the presence of inductive delays.

First, we examine the instability that arises when a constant power load is added to or removed from a network where the topology is unknown. While removing the dependence of the stability certificate on the interconnection structure creates a major technical challenge, it is beneficial as it allows for ease in network modification as the needs of a community vary. We thus develop conditions on individual power sources and loads such that a network comprised of many arbitrarily-connected units will be stable. We use Brayton-Moser potential theory to develop design constraints on individual microgrid components that certify transient stability—guaranteeing that the system will return to a suitable equilibrium after a change to the overall network loading. We find that stability can be guaranteed by installing a parallel capacitor at each constant power load, and we derive an expression for the required capacitance.

Second, we analyze the small-signal instabilities in microgrids containing arbitrary, rather than constant power, loads. This network representation allows for a more accurate representation of DC loads controlled by power converters which have a destabilizing negative incremental impedance over a finite frequency band in contrast to constant power loads which have a negative incremental impedance over all frequencies. While there are many established methods for the small-signal stability certification of DC networks, these methods do not explicitly account for the influence of network. In contrast, we develop a method for stability assessment of arbitrary DC grids by introducing the Augmented Power Dissipation and showing that it's positive definiteness is a sufficient condition for stability. We present an explicit expression for this quantity through load and network impedances and show how it could be directly used for stability certification of complex networks.

Thesis Supervisor: Konstantin Turitsyn
Title: Associate Professor, Department of Mechanical Engineering

Acknowledgments

First and foremost, I would like to thank my advisor, Professor Konstantin Turitsyn, for his help and guidance over the past two years. I am extremely grateful to have an advisor who is both profoundly curious and driven but also patient and kind. I came to graduate school a bit unfocused but with a powerful desire to learn and grow and I am thankful to have been afforded the opportunity to do that both through my research and through the freedom to take courses that interested me. Because of Professor Turitsyn, I have truly been able to achieve the growth I sought.

I have also been fortunate enough to find a supportive group of colleagues in Professor Turitsyn's lab including Dr. Petr Vorobev, without whom much of this thesis would not have been possible. Petr's curiosity is both admirable and contagious. I am exceedingly grateful for the time that Petr took, both over Skype and in person between sets of push ups, to explore concepts that puzzled me and to help me arrive at a stronger fundamental understanding.

Additionally, thank you to my friends, both new and old, for grounding me during this experience. I am grateful for the ability to have made life long friends battling through problem sets in the Mechanical Engineering department and exploring India with the Tata Center. I am also thankful for the powerful, fearless women of Barre&Soul Harvard Square who challenged my body and refreshed my spirit each time I stepped onto the mat. And, of course, thank you to my boyfriend Anders for his silliness, support and unwavering encouragement to follow what inspires me even if it does increase the number of miles between us.

Finally, to my biggest supporters, my parents: thank you for the wonderful life you fought to give me and the countless opportunities you have supported me through. I am grateful both for your encouragement of my baking habit and your dedication to picking up the phone every time I called with a new catastrophe or success. You go above and beyond and for that I am and will always be grateful.

Contents

List of Figures

List of Tables

Chapter 1

Introduction

1.1 Motivation: The Energy Access Gap

As of 2014, over 1 billion people, mainly in Sub-Saharan Africa and India, lack access to electricity. [12]. Electricity access is correlated with an increase on the Human Development Index and is critical to achieving many of the United Nations' Millenium Development Goals [21]. Specifically, energy access allows for poverty reduction through increased business opportunities, for increased education levels through the ability to study after dark and for improved health through more effective medical equipment and medication storage [28]. The access gap is even more apparent in rural areas where 27% lack electricity as compared to 4% in urban areas[3]. Solutions, tailored to the needs and ability to pay of these rural regions, are needed to bridge this gap. In many areas, grid extension is not practical financially or logistically. The International Energy Agency has suggested that the most cost effective way to electrify many of these areas is through decentralized systems powered by renewable energy resources such as solar or hydro power [12]. Therefore, local, off-grid solutions, such as village scale microgrids or household scale solar home systems, are an appropriate solution and have gained popularity.

1.2 DC Microgrids as a Solution

In the context of this work, we consider microgrids to be a collection of sources and loads which can operate independently. This definition varies slightly from that used in academic literature or by rural microgrid operators. First, many academic definitions of microgrids include the requirement that the system must be able to operate connected to a distribution grid. However, given the rural context considered for these networks and the lack of regulation in India to dictate how the interconnection of a microgrid and main grid would be realized, there is no explicit modeling of any interconnection structure in this work. Second, our definition allows for a broad variety of structures. In the context of India, most microgrids are structured with centralized generation from which the household loads are serviced. The definition provided allows for this structure but also allows for a broader analysis of more complex networks including but not limited to the interconnection of solar home systems which inherently include distributed generation resources. These types of topologies can provide numerous benefits to enhance the efficacy and utility of microgrids including added reliability and reduced storage costs due to power sharing between multiple generation or storage locations.

Both AC and DC microgrids can be implemented as off grid solutions. This thesis will focus explicitly on DC microgrids. While typical distribution grids and many existing microgrids carry alternating current, low-voltage DC microgrids have gained popularity in recent decades are appropriate in the rural or peri-urban environments where rates of energy access are the lowest [25]. A rigorous assessment presented in [14] assesses AC and DC grids on the merits of several criteria including generation and loading type, safety, stability, and size. In Sub-Saharan Africa and India, generation sources are typically solar panels which are inherently DC. Further, the storage devices used, lead acid or lithium batteries, are DC in nature as well. The recent improvement of power electronics has led to many relevant customer loads to become DC in nature, including fluorescent lights, computers and TVs [16]. An AC grid would require several inefficient conversions to accommodate the DC generation,

storage and loading. Additionally, since the villages in which these microgrids are deployed tend to be small having between 20 and 80 households [18] [19], low voltage networks can achieve appropriate efficiency and allow for greater ease in safety in operation as compared to MVDC or HVDC [13]. A final consideration is that AC grids are more difficult to stabilize and therefore to guarantee effective operation. Both AC and DC grids require voltage stabilization but AC grids require stabilization of frequency as well. While AC microgrids may be more common, the focus of this work on diminishing the energy access gap suggests that LVDC microgrids are more appropriate.

1.3 *Guaranteeing* Microgrid Stability

Microgrids can only be a solution to the energy access gap if they can operate reliably. It is important to note that there are two types of reliability related to the effective implementation of microgrids: service time and stability. Service time reflects the up-time of the grid, how often the grid can provide power. The quality of the service is dependent on the generation conditions, storage capacity and any optimal dispatch algorithms that may be in place. The focus of this thesis, however, is on the voltage stability of the network. Many optimal dispatch algorithms rely on the stable operation of the underlying network which in and of itself is a nontrivial problem. Therefore, we focus on guaranteeing the stability of the system to provide the groundwork on which increasingly efficient storage and generation as well as dispatch algorithms can improve the quality of service.

Within the context of the developing world, simple solutions that guarantee reliable and stable operation are more appropriate than complex control schemes. Simple solutions reduce system cost both with respect to hardware and upkeep, as a complex system requires a subject matter expert present for repairs. Therefore, this work focuses on the development of simple stability-aware design constraints. These constraints guide the development of individual units or the network as a whole. When satisfied, these constraints guarantee that the network will not experience voltage

collapse and thus can be utilized to its fullest.

While stability of DC networks has been studied extensively, many techniques require specific knowledge of loading or system structure. Deviations from the design of the network can compromise the results of these techniques. By developing design constraints on the basis of limited information about the loads and topology, uncertainty can easily be incorporated and the system operation made more robust. The guiding principle in the development of such robust design constraints is to define the worst-case configuration or situation for the instabilities studied. In this way, complex networks can be reduced to simple, more tractable systems that can be readily analyzed.

While there are a variety of instabilities that a DC microgrid can experience, this thesis will focus on developing system constraints that guarantee two types of stability, the load switching transient stability and small signal stability. The structure of this thesis is as follows. First we will present the notion of ad hoc microgirds, networks whose interconnection structure is not known a priori. We will leverage Brayton-Moser potential theory and Lyapunov analysis to examine a specific instability in these networks relating to the addition or removal of a constant power load from the network and define constraints on the network that will guarantee stability. Next, we broaden the load model to allow for a load with an arbitrary transfer function. We then propose a novel methodology to determine the small signal stability of a dc network which relies on the positivity of the Augmented Power Dissipationand the network structure itself. To show the utility of the certificate, several examples with different network topologies and loading are presented. This thesis will then summarize the conclusions reached and suggest paths for future work.

Chapter 2

Transient Stability of Ad Hoc DC Microgrids under Loading Variations

This chapter introduces the concept of an ad hoc microgrid and examines a specific large-signal instability associated with these networks. Ad hoc microgrids are microgrids that can operate in the absence of any knowledge of the network structure. Grids constructed in this manner can be strongly applicable to resource-constrained settings such as rebuilding communities after natural disasters or in the developing world where the energy access gap is still significant. This work will focus on the latter application where the low voltage DC architecture provides safety and easily interfaces with the DC based generation and storage [14]. In this context, ad hoc microgrids can be implemented in a variety of ways such as through the interconnection of independent solar home systems or through the development of energy access "kits" where each household would have its own set of outlets but share the generation resources of the village. In each of these cases, the addition or removal of a unit is simple in practice but could compromise the operation of the network. Therefore, the flexibility that the ad hoc microgrid architecture affords is critical because it ensures that the network can easily be modified to better meet the evolving needs of the community being served, thus reducing the amount of system planning required.

However, flexibility alone is not sufficient for operation. Reliable operation is critical for these networks to be used consistently and effectively. Certifying the

voltage stability of networks in the absence of a pre-deterined interconnection presents a unique but critical technical challenge for the development of these grids. There are two types of relevant instabilities in ad hoc microgrids. The first is the small signal instability which was addressed in [5]. The second, and the focus of this chapter, is the load switching instability. Due to the small size of the grids on which we are focusing, the addition or removal of a load to the network represents a significant change to the overall system loading which may result in voltage collapse. It is therefore necessary to certify the stability of a network to a family of loading variations.

This instability can only be observed when the system model reflects realistic implementations as it is a direct result of the interaction of the constant power loads with the resistive *and* inductive lines. In the absence of lines with some inductance, typical analysis would predict a stable reaction to a small load changing event as in Figure 2-1b even though, with realistic inductive lines as in Figure 2-1c, the voltage collapses given the same change in loading. While the destabilization mechanism due to the presence of inductive lines and a constant power load has been known in the power electronics community ([22, 1]), much of the previous literature in the power systems community ([24, 6, 26, 8, 4]) has considered purely resistive lines. Further, these works have considered networks with known topologies and the solutions presented do not easily extend to the arbitrary systems studied here.

While linear analysis techniques can be applied to small signal stability problems, the transient stability considerations, which are the focus of this chapter, tend to be more complicated because they require more sophisticated methodologies. [23] uses computational methods to address transient stability concerns with respect to self healing multiple-microgrid systems, which can reconfigure given an issue with a component microgrid with minimal loss of service. A MATLAB based time domain simulation is coupled with a JAVA framework for multi-agent systems for coordinated decision making. Conversely, a recent review [17] has focused on the importance of applying non-linear techniques to study transient stability with a specific focus on Lyapunov-based stability methods. The author notes that work has been undertaken regarding the stability of components, such as converters and induction loads; however

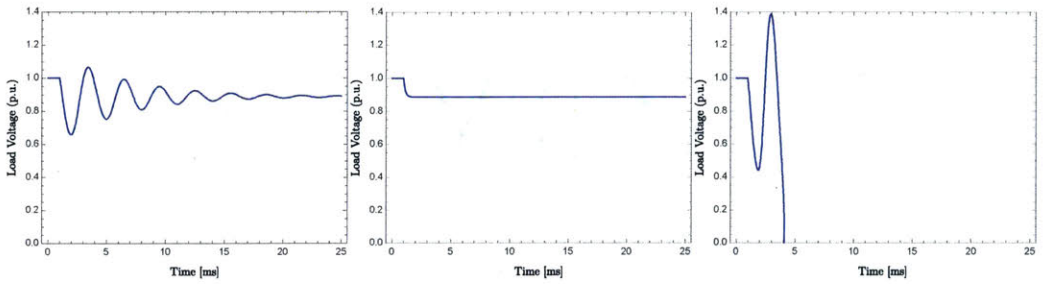

(a) τ = 1, C = 0.2 p.u. (b) τ = 0, C = 0.12 p.u. (c) τ = 1, C = 0.12 p.u.

Figure 2-1: Demonstration of load switching instability in a two-bus system

very little has been studied regarding the microgrid system as a whole. The authors believe that this area is not only important but has several pressing areas of research such as the comparison between small and large signal stability of a microgrid and the understanding of what operating conditions and system parameters could eliminate the region of attraction. Our work aligns with the gaps in scholarship identified and will focus on understanding the region of attraction and relevant parameters.

The layout of this chapter is as follows. First, we will establish component models and notation. Second, we will investigate the switching stability of a simple two bus system to establish the methodology used on a known system. Third, we present the abstraction to a grid with an unknown topology. Fourth, we present a general set of design constraints for the development of such networks. Finally, we assess the economic feasibility of this solution to guarantee the reliable operation of interconnected solar home systems in peri-urban areas of Africa and rural areas of India.

2.1 Models and Notation

In this section we present models for the interconnecting lines, power electronic loads, and voltage source converters which are analytically tractable and can be adapted to describe many networks. These are based on a previously presented ad hoc microgrid [13].

The electrical network is described as a weighted, directed graph $(\mathcal{V}, \mathcal{E})$ with a total of $|\mathcal{V}|$ nodes (buses) and $|\mathcal{E}|$ edges (lines). Each edge $\alpha \in \mathcal{E}$ represents a tuple

$\alpha = (i,j)$ with $i,j \in \mathcal{V}$. A power source or load is attached to each node and we denote the subset of vertex indices corresponding to loads as $\mathcal{L} \subset \mathcal{V}$ with and the subset of source indices as $\mathcal{S} \subset \mathcal{V}$. The state of the system is described by the voltage and current vectors $v \in \mathbb{R}^{|\mathcal{V}|}$ and $i \in \mathbb{R}^{|\mathcal{E}|}$. The topology of the graph is defined by the (transposed) incidence matrix $\nabla \in \mathbb{R}^{|\mathcal{E}|\times|\mathcal{V}|}$. Applying ∇ to the voltage vector results in a vector of potential differences across each line, and applying ∇^T to the current vector yields the total current flowing out of each node.

Each power line is associated with a graph edge $\alpha = (i,j) \in \mathcal{E}$ and is characterized by an inductance $L_\alpha = L_{ij}$ and a resistance $R_\alpha = R_{ij}$. Each line has time constant $\tau_\alpha = L_\alpha/R_\alpha$. Each line current i_α is described by:

$$L_\alpha \dot{i}_\alpha = -R_\alpha i_\alpha + \sum_{k\in\mathcal{V}} \nabla_{\alpha k} v_k, \quad \alpha \in \mathcal{E}. \tag{2.1}$$

Load k is represented by the parallel connection of a capacitance C_k and a constant power load drawing power p_k. In general, constant power loads represent perfectly-regulated power converters with constant resistance loads, and hence are conservative and general models which can be used to describe many power electronic devices. The dynamics of these converters are much faster than the inductive response of the lines. The capacitor across the input of the power converter is a standard feature, and is critical for system stability [8]. Each load voltage is described by:

$$C_k \dot{v}_k = -\frac{p_k}{v_k} - \sum_{\alpha\in\mathcal{E}} \nabla_{\alpha k} i_\alpha, \quad k \in \mathcal{L}. \tag{2.2}$$

In this work we assume the source controller, which regulates the converter output voltage, has dynamics much faster than the network. Accordingly, we model them as perfect voltage sources: $v_k = V_0, \quad k \in \mathcal{S}$. The extension to controllable converters with proportional (droop) and integral voltage control is relatively straightforward [5]. A summary of the component models considered for the ad hoc microgrid networks is given in Figure 2-2.

Characterizing system stability requires a suitable family of Lyapunov (potential) functions. Extrema of a particular potential correspond to equilibria of the system,

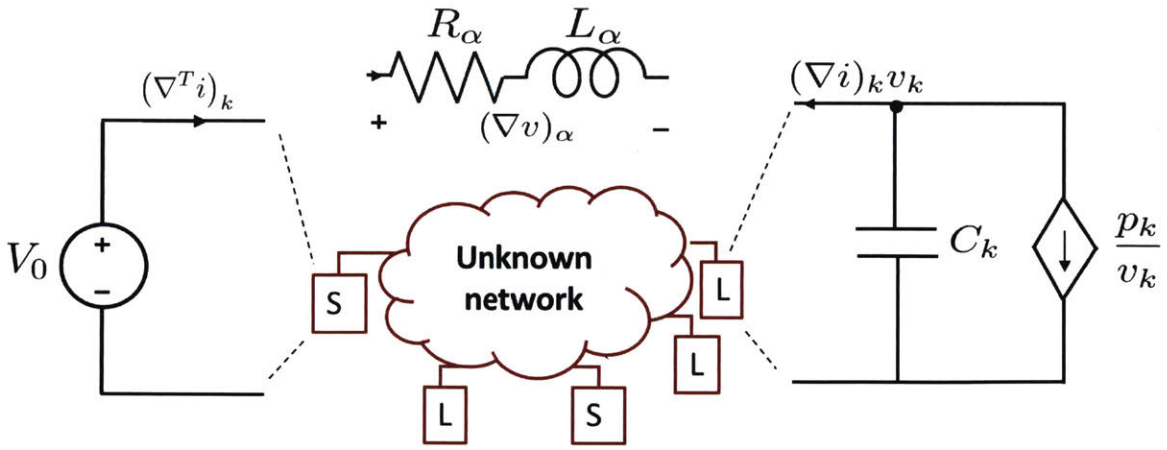

Figure 2-2: Ad hoc microgrid

and stability can be certified by demonstrating certain properties of the potential. Unfortunately, the presence of constant power loads and lack of global stability in power systems preclude the use of potential functions based on system energy (Hamiltonian potentials). However, the seminal results of Brayton and Moser are applicable to our setting [7, 15]. The Brayton Moser potential represents the system dynamics in a quasi-gradient form ($\mathcal{Q}\dot{x} = -\partial_x \mathcal{P}$), which is particularly useful for certification of transient stability. Whenever the matrix $\mathcal{Q}$ is positive definite in some region, the potential $\mathcal{P}$ is a non-increasing function: $\dot{\mathcal{P}} = -\dot{x}^T \mathcal{Q}\dot{x}$. Lower and upper bounds on $\mathcal{P}$ that hold for arbitrary networks can be used to establish stability for ad hoc networks.

For our architecture, a representation with the proper structure (derived in [5]) is given by:

$$\mathcal{G}(v) = \sum_{(i,j)\epsilon\mathcal{E}} \frac{(v_i - v_j)^2}{2R_{ij}} + \sum_{k\epsilon\mathcal{L}} p_k \log v_k \tag{2.3}$$

$$\mathcal{P}(x) = \mathcal{G}(v) + \frac{1}{2}\sum_{\alpha\epsilon\mathcal{E}} (\tau_{\max} - \tau_\alpha) L_\alpha \dot{i}_\alpha^2 + \frac{\tau_{\max}}{2} \sum_{k\epsilon\mathcal{L}} C_k \dot{v}_k^2 \tag{2.4}$$

$$\mathcal{Q} = \begin{bmatrix} \operatorname{diag}(\tau_{\max} R_\alpha - L_\alpha) & -\tau_{\max} \nabla_{\mathcal{E}\mathcal{L}} \\ \tau_{\max} \nabla_{\mathcal{E}\mathcal{L}}^T & \operatorname{diag}\left(C_k - \tau_{\max} \frac{p_k}{v_k^2}\right) \end{bmatrix} \tag{2.5}$$

x is the state vector $[i_{\mathcal{E}}^T, v_{\mathcal{L}}^T]^T$ and $\dot{i}_\alpha$, $\dot{v}_k$ are given in Eqs. (2.1) and (2.2). $\tau_{\max}$ is an upper bound on the line time constants in the network—for convenience, we define it to be strictly larger than the largest time constant: $\tau_{\max} > \max_\alpha \tau_\alpha$. $\nabla_{\mathcal{EL}}$ refers to the submatrix of ∇ corresponding to the load nodes. Finally, in addition to being notationally convenient, $\mathcal{G}$ is well-studied and is referred to in the literature as the resistive co-content [15]. It is also worth noting, that all equilibria of the system correspond to extrema of $\mathcal{P}$, and vice-versa, every extremum of $\mathcal{P}$ to an equilibrium of the system. Moreover, the extrema of the potential $\mathcal{G}(v)$ correspond to the solutions of the equilibrium power flow equations.

2.2 Load-Switching Stability of a Two Bus System

In this section we consider the two bus system shown in Figure 2-3a, to provide a simple introduction to the techniques we will use in the next section to analyze ad hoc networks with no topology constraints. The dynamic equations of the system are given by:

$$C\dot{v} = -\frac{p}{v} + i \tag{2.6}$$

$$L\dot{i} = -Ri + V_0 - v\,. \tag{2.7}$$

The relationship between the voltage v at the load and the load magnitude p at equilibrium (the "nose curve") is shown in Figure 2-3b. The largest load that can be supported is the apex of the nose curve at $p = P_0 = V_0^2/4R$, which corresponds to a load bus voltage of $V_0/2$. For all $p < P_0$, there are two solutions:

$$V_{\text{high}}(p, R) = \tfrac{V_0}{2}\left(1 + \sqrt{1 - \tfrac{p}{P_0(R)}}\right) \tag{2.8}$$

$$V_{\text{low}}(p, R) = \tfrac{V_0}{2}\left(1 - \sqrt{1 - \tfrac{p}{P_0(R)}}\right) \tag{2.9}$$

where V_{high} and V_{low} are the high and low equilibrium points. When the power exceeds

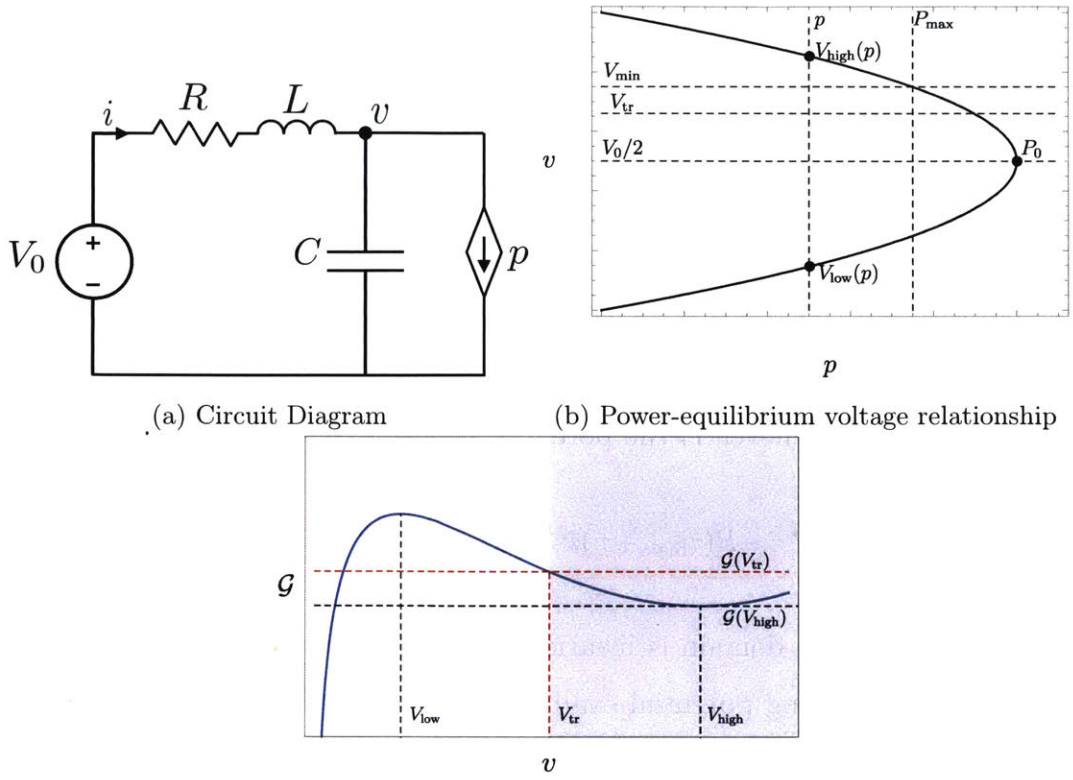

(a) Circuit Diagram

(b) Power-equilibrium voltage relationship

(c) Resistive co-content

Figure 2-3: Two Bus System

P_0, $\mathcal{G}$ does not have any extrema and the system has no equilibria. For the network to achieve a minimum voltage of $V_0 > V_{\min} > V_0/2$, the largest load that can be supported is $P_{\max} = V_{\min}(V_0 - V_{\min})/R$.

To analyze transient stability, we first define a "switching event" to be any time t such that the load power changes instantaneously:

$$p(t^-) \neq p(t^+)\,. \tag{2.10}$$

Hereafter, $^+$ and $^-$ refer to quantities evaluated at t^+ and t^-. All state variables are continuous: $i^- = i^+$ and $v^- = v^+$. We assume that the system is at equilibrium before the switching event: $v^- = V_{\text{high}}^-$.

Applying the definitions of $\mathcal{G}$ and $\mathcal{P}$ from Sec. 2.1 yields:

$$\mathcal{G}(v) = \frac{(V_0 - v)^2}{2R} + p \log v \tag{2.11}$$

$$\mathcal{P}(x) = \mathcal{G} + \frac{1}{2}(\tau_{\max} - \tau) L \dot{i}^2 + \frac{\tau_{\max}}{2} C \dot{v}^2 . \tag{2.12}$$

The resistive co-content $\mathcal{G}$ for a two bus system is given in Figure 2-3c. According to Lyapunov's theorem, convergence to a stable equilibrium point after a switching event is guaranteed whenever 1) the potential $\mathcal{P}$ is strictly decreasing with time:

$$\dot{\mathcal{P}} = -R(\tau_{\max} - \tau)\dot{i}^2 - \left(C - \frac{\tau_{\max} p}{v^2}\right) \dot{v}^2 < 0, \tag{2.13}$$

and 2) the high voltage domain is invariant and contains a single equilibrium point and 3) the post switching potential evaluated at the pre-switching equilibrium, due to the continuity of state variables, is less than the potential of the bound on the voltage domain: $\mathcal{P}^+(V_{\text{high}}^-) < \mathcal{P}^+(V_{\text{tr}})$.

To satisfy the first requirement, we note that the first term of Equation (2.13) is negative by definition. Therefore, to ensure the second term is also negative, a lower bound on the load bus voltage during transients, denoted by V_{tr}, is imposed such that $v \geq V_{\text{tr}}$. The choice of V_{tr} provides a bound on C such that

$$C > \frac{\tau P^{\max}}{V_{\text{tr}}^2} \tag{2.14}$$

To satisfy the second requirement, we must choose V_{tr} such that the stable equilibrium point is in the domain and the unstable point, in a two bus system V_{low}, is not. Therefore the value of V_{tr} is bounded from above by $V_{\min}$, the lowest acceptable equilibrium point, and from below by V_{low}. For simplicity, we impose a stricter lower bound of $V_0/2$. V_{tr} is thus bounded such that $V_{\min} \geq V_{\text{tr}} \geq V_0/2$.

The third requirement can be simplified given that $\mathcal{P}^+(V_{\text{tr}})$ is bounded from below by $\mathcal{G}^+(V_{\text{tr}})$ such that

$$\mathcal{P}^+(V_{\text{high}}^-) < \mathcal{G}^+(V_{\text{tr}}) \tag{2.15}$$

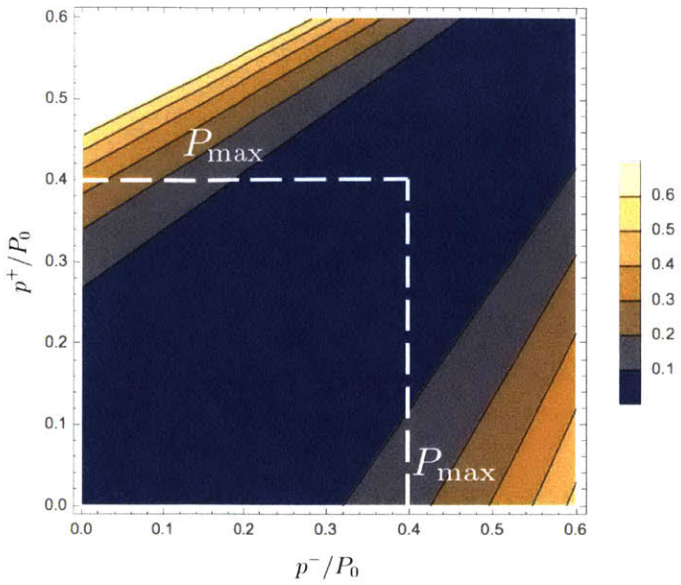

Figure 2-4: Level sets of capacitance (normalized by $C_0 = \tau/R$) required for a load variation from p^- to p^+. The bounds on loading are indicated by $P_{\max}$

The transient component of $\mathcal{P}$ can be expressed in terms of the state variables by characterizing the capacitor current as $C\dot{v}(t^+) = (p^- - p^+)/V^-_{\text{high}}$. which then yields

$$\mathcal{P}^+ = \mathcal{G}^+(V^-_{\text{high}}) + \frac{\tau}{2C}\left(\frac{p^- - p^+}{V^-_{\text{high}}}\right)^2 . \tag{2.16}$$

This representation of $\mathcal{P}$ makes explicit that larger values of C decrease the total potential. Therefore, the third stability condition yields a bound $C > C_{\text{tr}}(p^-, p^+)$ where C_{tr} is given by:

$$C_{\text{tr}}(p^-, p^+) = \frac{\tau}{2(\mathcal{G}^+(V_{\text{tr}}) - \mathcal{G}^+(V^-_{\text{high}}))}\left(\frac{p^- - p^+}{V^-_{\text{high}}}\right)^2$$

This expression can be reduced to a minimum capacitance bound, which is analogous to Eq. (2.14) and removes the direct dependence on p^- and p^+, by characterizing the "worst-case" switching event $p^- \to p^+$

$$
\begin{aligned}
C > \max_{p^-,\, p^+} \; & C_{\mathrm{tr}}\left(p^-, p^+\right) \\
\text{subject to} \quad & p^- \le P_{\max} \\
& p^+ \le P_{\max}
\end{aligned}
\tag{2.17}
$$

The sufficient condition on capacitance is given when both Eqs. (2.14) and (2.17) are satisfied. This optimization problem can easily be solved computationally to provide a lower bound on the parallel load capacitance.

2.3 Generalization to Networks

In this section we generalize our analysis to arbitrary networks, in the absence of any restrictions on topology. We begin with a few simple assumptions. First, we assume our network has one strongly-connected component with at least one source. Second, all sources are assumed to be perfectly regulated with a voltage of V_0. Third, we assume that the aggregate resistance of all lines is bounded from above by $\sum_{(i,j)\in\mathcal{E}} R_{ij} \le R_{\max}$. Fourth, we define system loadability, p_Σ, as the instantaneous sum of constituent loads such that $p_\Sigma = \sum_{k\in\mathcal{L}} p_k$ and assume it is bounded from above by $P_{\max}$: $p_\Sigma \le P_{\max} < P_0 = V_0^2/4R_{\max}$. The maximum system loadability is bounded by P_0 of the equivalent two-bus network. Fifth, we assume a single lower bound across all buses for the equilibrium voltage and voltage during transients given by scalars $V_{\min}$ and V_{tr}, respectively. While traditional design practices for known networks may benefit from using non-uniform voltage constraints, the consideration of an arbitrary network without knowledge of of specific loads lends itself toward utilizing consistent bounds across all buses. Finally, the power consumption of each load is bounded from above by $p_k^{\max}$, $p_k \le p_k^{\max}$, which can vary between loads.

The rest of the section is organized as follows. After brief review of the previously established conditions for existence of equilibrium (Lemma 1), we show that for any network the potential $\mathcal{P}$ can serve as a valid Lyapunov function (Corollary 1 and Lemma 2). We then establish the invariant sublevel set of $\mathcal{P}$ (Theorem 2) and estimate the value of $\mathcal{P}$ after an arbitrary switching event in Lemma 4. Combination

of these results allows us to formulate the central condition (2.29) on the capacitance guaranteeing the stability of the system.

We start by introducing the high voltage equilibrium voltage profile v^{sep} and equilibrium state $x^{\text{sep}} = [(i^{\text{sep}})^T, (v_{\mathcal{L}}^{\text{sep}})^T]^T$ where $i^{\text{sep}} = \text{diag}(R_k^{-1})\nabla v^{\text{sep}}$. Existence and uniqueness of this equilibrium is guaranteed by the following Lemma [27]:

Lemma 1 *Whenever $p_\Sigma < P_0$, there exists exactly one solution to the power flow equations $\partial_v \mathcal{G} = 0$ with all load buses satisfying $v_k > V_{\text{high}}(p_\Sigma, R_{\max})$. At the same time, all other equilibria have at least one load bus $\kappa \in \mathcal{L}$ such that $v_\kappa < V_{\text{low}}(p_\Sigma, R_{\max})$.*

Proof 1 *See [27], Supplementary Theorem 1.*

The quantities V_{low} and V_{high} are scalar functions defined in Equations (2.8) and (2.9). The bounds established in Lemma 1 demonstrate that exactly one feasible equilibrium point is guaranteed to exist for any $p_\Sigma \leq P_{\max}$ if and only if $R_{\max}$, $P_{\max}$, $V_{\min}$, and V_0 satisfy $V_{\text{high}}(P_{\max}, R_{\max}) \geq V_{\min}$ with V_{high} given by Eq. (2.8). This condition is equivalent to

$$P_{\max} \leq \frac{V_{\min}(V_0 - V_{\min})}{R_{\max}}. \tag{2.18}$$

Both inequalities in Lemma 1 become tight for the two-bus system—in this sense, the two bus topology (one source separated from multiple loads with total power p_Σ by a line of resistance $R_{\max}$) is the "worst-case" topology for equilibrium point feasibility. This also implies that condition (2.18) is both necessary and sufficient for existence of a feasible equilibrium in an ad hoc setting.

Theorem 1 *The function $\mathcal{G}(v)$ is strictly convex whenever all load voltages satisfy $v_k > V_0/2$ and $p_\Sigma < P_0$.*

Proof 2 *The quadratic form of the Hessian is given by*

$$w^T \partial_{vv} \mathcal{G}(v) w = \sum_{(i,j)\in\mathcal{E}} \frac{(w_i - w_j)^2}{R_{ij}} - \sum_{k\in\mathcal{L}} \frac{p_k}{v_k^2} w_k^2, \tag{2.19}$$

where we formally define $w_k = 0$ *whenever* $k \in \mathcal{S}$. *For* $k \in \mathcal{L}$, *let* Π_k *be a path connecting bus* k *to one of the sources. Then* $w_k = \sum_{(i,j)\in\Pi_k}(w_i - w_j)$. *Define* $R_{\Pi_k} = \sum_{(i,j)\in\Pi_k} R_{ij}$. *The term* w_k^2 *in* (2.19) *can be then bounded with the help of Jensen's inequality as*

$$\begin{aligned} w_k^2 &= \left(\sum_{(i,j)\in\Pi_k}(w_i - w_j)\right)^2 \\ &= R_{\Pi_k}^2 \left(\sum_{(i,j)\in\Pi_k} \frac{R_{ij}}{R_{\Pi_k}} \frac{w_i - w_j}{R_{ij}}\right)^2 \\ &\le R_{\Pi_k}^2 \sum_{(i,j)\in\Pi_k} \frac{R_{ij}}{R_{\Pi_k}} \left(\frac{w_i - w_j}{R_{ij}}\right)^2 \\ &\le R_{\max} \sum_{(i,j)\in\Pi_k} \frac{(w_i - w_j)^2}{R_{ij}} \end{aligned}$$

Hence, for the Hessian quadratic form we have

$$\begin{aligned} w^T \partial_{vv}\mathcal{G}(v) w &> \sum_{(i,j)\in\mathcal{E}} \frac{(w_i - w_j)^2}{R_{ij}} \left(1 - \sum_{k:(i,j)\in\Pi_k} \frac{p_k R_{\max}}{v_k^2}\right) \\ &> \sum_{(i,j)\in\mathcal{E}} \frac{(w_i - w_j)^2}{R_{ij}} \left(1 - \frac{4p_\Sigma R_{\max}}{V_0^2}\right) > 0 \end{aligned}$$

Corollary 1 *The voltage profile* v^{sep} *minimizes the function* $\mathcal{G}$ *in the domain* $v_k > V_0/2$ *for* $k \in \mathcal{L}$. *Furthermore in the same domain, and for arbitrary currents, we obtain* $\mathcal{P}(x) > \mathcal{G}^{\text{sep}} = \mathcal{G}(v^{\text{sep}})$ *whenever* $x \neq x^{\text{sep}}$ *and* $\mathcal{P}(x) = \mathcal{G}^{\text{sep}}$ *for* $x = x^{\text{sep}}$.

Next, we identify the conditions for the decay of the Lyapunov function $\mathcal{P}$ in the transiently acceptable domain of $\mathcal{T} = \{x : v_k > V_{\text{tr}} > V_0/2\}$.

Lemma 2 *Whenever the capacitances on all the load buses satisfy*

$$C_k > \frac{\tau p_k^{\max}}{V_{\text{tr}}^2}, \tag{2.20}$$

one has $\dot{\mathcal{P}} < 0$ *whenever* $x \in \mathcal{T} \setminus \{x^{\text{sep}}\}$.

Proof 3 *This result follows directly from the relation* $\dot{\mathcal{P}} = -\dot{x}^T \mathcal{Q} \dot{x}$ *and positive definiteness of the matrix* $\mathcal{Q}$ *as defined in equation* (2.5).

These two results imply that any sublevel set of $\mathcal{P}$ inside $\mathcal{T}$ is invariant and any trajectory starting inside such a sublevel set converges to the equilibrium point x^{sep}. These sublevel sets are compact as the function $\mathcal{P}$ is bounded from below by a convex $\mathcal{G}$. To estimate the largest sublevel set of $\mathcal{P}$ that is contained in the transient domain $\mathcal{T}$ we prove the following theorem.

Theorem 2 *The function $\mathcal{P}$ evaluated at the boundary $\partial\mathcal{T}$ is bounded from below such that $\mathcal{P}(x) \geq \mathcal{G}^{+}_{\text{tr}}$ where*

$$\mathcal{G}^{+}_{\text{tr}} = \frac{(V_{\text{tr}} - V_0)^2}{2R_{\max}} + p^{+}_{\Sigma} \log V_{\text{tr}} \tag{2.21}$$

Proof 4 *Given $\mathcal{P} \geq \mathcal{G}$, it is sufficient to establish the bound on $\mathcal{G}$. Given that $x \in \partial\mathcal{T}$, there exists a load bus κ with $v_\kappa = V_{\text{tr}}$. Consider a path $\Pi \subset \mathcal{E}$ connecting the bus κ to some source in the system and define $R_\Pi = \sum_{(i,j)\in\Pi} R_{ij}$ Applying the same Jensen's inequality approach as in Theorem 1, we show that the potential $\mathcal{G}$ satisfies*

$$\begin{aligned}
\mathcal{G}(v) &= \sum_{(i,j)\in\mathcal{E}} \frac{(v_i - v_j)^2}{2R_{ij}} + \sum_{i\in\mathcal{L}} p_i \log v_i \\
&\geq \sum_{(i,j)\in\Pi} \frac{(v_i - v_j)^2}{2R_{ij}} + \sum_{i} p_i \log V_{\text{tr}} \\
&\geq \frac{(v_\kappa - V_0)^2}{2R_\Pi} + p_\Sigma \log V_{\text{tr}} \\
&\geq \frac{(V_{\text{tr}} - V_0)^2}{2R_{\max}} + p_\Sigma \log V_{\text{tr}}
\end{aligned}$$

To certify transient stability of the system after the switching event, we estimate the corresponding value of the Lyapunov function $\mathcal{P}$. Specifically we consider an event when only one of the loads $\kappa \in \mathcal{L}$ experiences switching, changing its power from p^{-}_κ to p^{+}_κ.

Lemma 3 *At any equilibrium point, the potential $\mathcal{G}$ can be represented as*

$$\mathcal{G}(v) = \sum_{i\in\mathcal{L}} \left[\frac{p_i}{v_i} \frac{(V_0 - v_i)}{2} + p_i \log(v_i) \right] \tag{2.22}$$

Proof 5 *Assume that i_k with $k \in \mathcal{V}$ are the nodal currents leaving the sources or the*

loads. The global current conservation law implies that

$$\sum_{k\in\mathcal{S}} i_k = -\sum_{k\in\mathcal{L}} i_k \tag{2.23}$$

On the other hand, whenever the voltage on all the source buses is given by V_0*, and there is no capacitor charging/discharging current at equilibrium, it follows from the energy conservation that the energy produced by the sources is equal to energy consumed by the loads plus the energy dissipated in the lines, or more formally*

$$\sum_{k\in\mathcal{S}} i_k V_0 = -\sum_{k\in\mathcal{L}} i_k v_k + \sum_{(i,j)\in\mathcal{E}} \frac{(v_i - v_j)^2}{R_{ij}} \tag{2.24}$$

Combining the definition (2.3) *with the relations* (2.23) *and* (2.24) *one arrives at* (2.22).

Lemma 4 *For a single load switching event in a network initially at equilibrium, where only one load* $\kappa \in \mathcal{L}$ *changes, the following bound holds for the potential* $\mathcal{P}$*:*

$$\mathcal{P}(x(t^+)) \le \mathcal{G}^+_{\text{ini}} + \frac{\tau_{\max}}{2C_\kappa}\left(\frac{p^-_\kappa - p^+_\kappa}{V^-_{\text{high}}}\right)^2 \tag{2.25}$$

$$\mathcal{G}^+_{\text{ini}} = \frac{p^-_\Sigma}{2}\frac{V_0 - V^-_{\text{high}}}{V^-_{\text{high}}} + p^+_\Sigma \log V_0 \tag{2.26}$$

Proof 6 *We start by bounding the* $\mathcal{G}(v(t^+))$*. Noting that Lemma 1 defines the lower bound of voltage level* $v_k \ge V_{\text{high}}(p^-_\Sigma)$*, while the upper bound is* $v_k \le V_0$*, we use the expression* (2.22) *in Lemma 3 to obtain the following bound:*

$$\begin{aligned}
\mathcal{G}^+(v(t^-)) &= \sum_{i\in\mathcal{L}}\left[\frac{p^-_i}{v^-_i}\frac{(V_0 - v^-_i)}{2} + p^+_i \log(v^-_i)\right] \\
&\le \frac{V_0 - V^-_{\text{high}}}{2V^-_{\text{high}}}\sum_{i\in\mathcal{L}} p^-_i + \log(V_0)\sum_{i\in\mathcal{L}} p^+_i \\
&\le \frac{p^-_\Sigma}{2}\frac{V_0 - V^-_{\text{high}}}{V^-_{\text{high}}} + p^+_\Sigma \log(V_0)
\end{aligned} \tag{2.27}$$

Next, due to the continuity of the state variables, and relation (2.1)*, one has* $L\dot{i}(t^-) = L\dot{i}(t^+) = 0$*, so only the terms involving* $\dot{v}$ *change after switching. Given that* $p_k \ge 0$

for all $k \in \mathcal{L}$ *and* $\dot{v}_k = 0$ *for* $k \neq \kappa$ *we obtain.*

$$\begin{aligned}\frac{\tau_{\max}}{2}\sum_{k\in\mathcal{L}} C_k \dot{v}_k^2 &= \frac{\tau_{\max}}{2}\frac{1}{C_\kappa}\left(-\frac{p_\kappa^+}{v_\kappa^-} - \sum_{\alpha\in\mathcal{E}} \nabla_{\alpha\kappa} i_\alpha\right)^2 \\ &\leq \frac{\tau_{\max}}{2C_\kappa}\left(\frac{p_\kappa^- - p_\kappa^+}{v_\kappa^-}\right)^2 \\ &\leq \frac{\tau_{\max}}{2C_\kappa}\left(\frac{p_\kappa^- - p_\kappa^+}{V_{\text{high}}^-}\right)^2 \end{aligned} \tag{2.28}$$

Combining the bounds (2.28) *with* (2.27) *we arrive at* (2.25).

Theorem 3 *The system starting at stable equilibrium and experiencing an arbitrary single-load switching event returns back to a stable equilibrium point whenever the capacitors installed on every load satisfy both Equation* (2.20) *and:*

$$C_\kappa > \max_{p_\Sigma^-,\, p_\Sigma^+} \frac{\tau_{\max}}{2\left(\mathcal{G}_{\text{tr}}^+ - \mathcal{G}_{\text{ini}}^+\right)}\left(\frac{p_\Sigma^- - p_\Sigma^+}{V_{\text{high}}^-}\right)^2 \tag{2.29}$$

$$\begin{aligned} \text{subject to} \quad & p_\Sigma^- \leq P_{\max} \\ & p_\Sigma^+ \leq P_{\max} \\ & |p_\Sigma^+ - p_\Sigma^-| \leq p_\kappa^{\max} \end{aligned}$$

Proof 7 *This result is proven by combining all previous bounds. Specifically, the condition* (2.29) *ensures that the value of the post-switch potential function* $\mathcal{P}(x(t^+))$ *estimated in* (2.25) *is less than* $\mathcal{G}_{\text{tr}}^+$ *defined in* (2.21), *which is the minimal value of the potential that any network can achieve within the transiently acceptable domain* $\mathcal{T}$. *Temporal decay of* $\mathcal{P}$ *established by Lemma 2 under assumption* (2.20) *implies that the system will stay inside* $\mathcal{T}$. *Therefore, in accordance to Lyapunov theorem, positive-definiteness of* $\mathcal{P}(x) - \mathcal{G}^{\text{sep}}$ *(Corollary 1) and its temporal decay (Lemma 2) inside* $\mathcal{T} \setminus \{x^{\text{sep}}\}$ *implies that the system will converge to* x^{sep}.

Remark 1 *For each* V_{tr}, *the sufficient bound for* C *defined by* (2.29) *exists only for small enough values of power,* $p_\kappa^{\max} \leq P_\kappa^{\text{crit}}$. *Above those levels, stability cannot be certified for any capacitance as the initial energy* $\mathcal{G}_{\text{ini}}^+$ *may exceed* $\mathcal{G}_{\text{tr}}^+$ *for some admissible values of* p_Σ^-, p_Σ^+.

Remark 2 *Numerical simulation demonstrates that the worst case switching scenario (the scenario that maximizes $C_{\kappa,\mathrm{tr}}$) corresponds to $p_\Sigma^- = P_{\max} - p_\kappa^{\max}$ and $p_\Sigma^+ = P_{\max}$, that is load κ switching on to its maximum power and bringing the total network loading to $P_{\max}$.*

The nature of the derivation above implies that the condition (2.29) is sufficient but not necessary. The following Lemma introduces a necessary condition:

Lemma 5 *For a system to maintain stability in an ad hoc setting, it is necessary that each load capacitance satisfies*

$$C_\kappa > \frac{\tau p_k^{\max}}{V_{\min}^2} \tag{2.30}$$

Proof 8 *As follows from the discussion in section 2.2, violation of this condition results in the loss of asymptotic stability for a two-bus system with load power $p^{\max} = P_{\max}$.*

Tighter necessary conditions (not shown) can be obtained numerically by simulating transients in specific networks, and these conditions are in close agreement with (2.30).

2.4 Discussion

A comparison of the lower bounds on C, normalized by $C_0 = \tau_{\max}/R_{\max}$, during a switching event, whose magnitude is normalized by the natural unit of power $P_0 = V_0^2/4R_{\max}$, is presented in Figure 2-5. The larger the load, the larger the capacitance required to ensure stability. The small signal stability constraint (Eq. (2.30)) is a necessary condition while the transient stability constraint (Eqs. (2.20) and (2.29)) is a sufficient condition. The gap between these constraints gives an indication of how conservative the sufficient bounds are.

The choice of V_{tr} alters the capacitance constraints. Increasing the levels of V_{tr} decreases the requirements imposed by Eq. (2.20) but increases the ones from (2.29). Furthermore, high levels of V_{tr} result in relatively small critical levels of load power

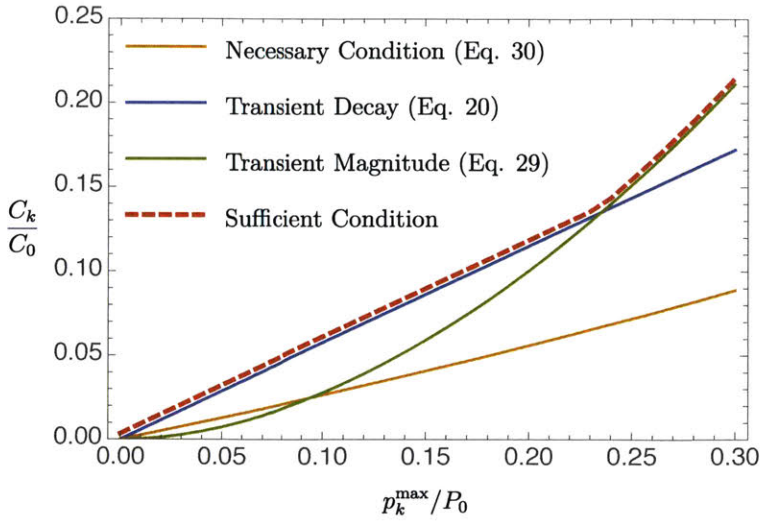

Figure 2-5: Comparison of lower bounds on C_k/C_0 for $V_{\text{tr}} = 0.66V_0$.

as discussed in Remark 1. For example, given $V_{\text{tr}} = 0.66V_0$ as in Figure 2-5, the maximum load power consumption is $P_\kappa^{\text{crit}} \approx 0.47P_0$. A trade-off, shown in Figure 2-6, therefore exists between power demanded and magnitude of the capacitance as well as between choice of V_{tr} and P_k^{crit}.

2.5 Proposed Design Scheme

We have established a lower bound on load capacitance which can guarantee network stability without pre-determining the network topology. Our bound provides a theoretical foundation for ad hoc microgrids with modular source and load units. The development process for these microgrids is

1. Define acceptable voltage levels across all units based on converter constraints: nominal voltage V_0, minimal acceptable equilibrium voltage $V_{\min}$, minimum acceptable voltage during switching transients V_{tr}.

2. Select system parameters: the upper bound on system loading $P_{\max}$ and the maximum line resistance $R_{\max}$ (determined by line material, diameter and length).

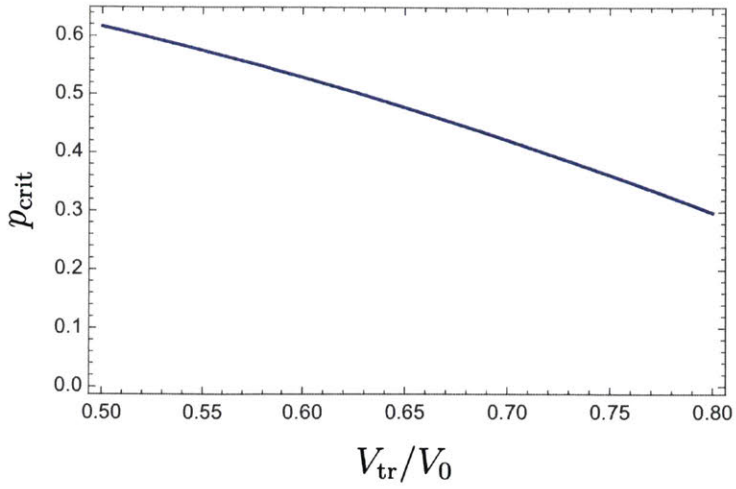

Figure 2-6: The relationship between the maximum node power for which the network can be guaranteed stable as a function of the minimum allowable voltage V_0.

3. For each load κ with maximum power $p_\kappa^{\max}$, select a capacitance that ensures stability according to the constraints in Figure 2-5.

This process is independent of the network topology and therefore it does not need to be repeated for each community. Instead, it can be performed once to develop units that could be produced in bulk and easily adapted to the changing needs of individual communities without oversight.

2.6 Practical Implementation: A Techno-Economic Model of Interconnected Solar Home Systems in India and Sub-Saharan Africa

Many off grid technologies tend to exist in isolation, such as single household solar home systems or single village microgrids. There is potention in the interconnection of these systems but, with interconnection, comes the risk of instabilities. The work presented her on quantifying the necessary capacitance for system stability can allow interconnection while guaranteeing stability. The interconnection of solar home systems is a prudent case study due to the presence of distributed energy resources and

the small distance between households in contrast to microgrids which tend to be in isolated areas such that the cost to connect them is prohibitive.

There are several manners for these companies to benefit from interconnected SHS. First, they can reduce the required storage with little impact on the reliability. Second, these companies can charge increased tariffs that the customers can offset through peer-to-peer energy trading. Finally, the payback period for the SHS can decrease due to the increased tariffs. This is beneficial for the company because it reduces the likelihood that the customers will default and it benefits the end user by allowing them to own their own system more quickly, accruing less interest.

2.6.1 Techno-Economoic Model (TEM) Description

This model compares the return on investment (ROI) for isolated solar home systems with that of interconnected systems. The inputs required for this analysis are given in Tables 2.1 and 2.2 for the isolated systems and interconnected systems, respectively. The parameters are divided into three categories: capital expenses, service income and physical system parameters.

The model constructed for the isolated solar system is relatively simple. The storage per household is assumed to be consistent in the village. The capital expenditure considers only the storage and the hardware cost (which is comprised of the load unit and the solar panel and evaluated based on the size of the solar panel). For service, a monthly tariff is assessed and the battery lifetime is taken into account by incrementing the storage component of the capital expenditure after the lifetime is completed. It is assumed that if the village becomes profitable before the battery lifetime they will be responsible for the purchase of new batteries.

The model for the interconnected solar home systems is more complex. The capital expenditures contain the same contributions from hardware and storage, but there is also an added contribution from the cables required to interconnect the SHS and the stabilizing capacitors. The cables considered here are less expensive than typical cables used in microgrids and therefore could not be assumed to be grid compatible. The amount of storage required is assessed in terms of a percent decrease from the

	Variable	Approx Value Range	Simulation Value
Capital	Storage(Ah/household)	10-20	15
	Cost of Storage ($/Ah)	2-3	2.2
	Number of Homes	10-70	60
	Hardware Cost($/W)	1.05	1.05
Service	Monthly Tariff - India ($)	2-5	2
	Monthly Tariff - Africa ($)	10-15	10
	Battery Lifetime (yr)	2-7	5
System	Solar Panel (W)	150	150

Table 2.1: Isolated SHS Input Variables

nominal amount required for the isolated solar homes. Further, there are two tiers for service: one for normal loads, those in the linear range of Figure 2-5 and one for larger loads, those in the superlinear range. These loading levels are defined in terms of the upper bound on their power consumption. The monthly tariff for these tiers is given in terms of percent increase from the nominal tariff. Finally, the system parameters such as battery voltage, line resistance, line time constant, minimum voltage and total aggregate power demand are included as they are required for the calculation of the minimum capacitance.The output was chosen to be the return on investment because the SHSs are typically more expensive then ability to pay of the target consumers. Therefore, companies tend to be more concerned with how long it will take customers or villages to pay back their investment.

2.6.2 TEM Limitations

A primary assumption of this model is that reliability of the system is valued. The value of reliability is a key component to increasing the monthly tariffs but the quantification of this value was not investigated for this model. Additionally, labor costs are not explicitly considered in this analysis; however, they are be assumed to be incorporated into the cost of the hardware. The loading used in this model is very simplified. Two basic categories of loads are assumed, defined by their maximum power consumption. The implication is that, for appliances which consume less power than those levels, the capacitance estimated is larger than what is required to cer-

	Variable	Value Range	Simulation Value
Capital	Nominal Storage(Ah/household)	10-20	15
	Cost of Storage ($/Ah)	2-3	2.2
	Reduction in Storage (%)	10-40	20
	Cable Cost ($/km)	2000-3000	2000
	Interconnection Distance (km)	0.25-2.0	1.28
	Total Number of Homes	10-70	60
	Number of Homes- Large Loads	2-6	4
	Hardware Cost($/W)	1.05	1.05
	Stabilizing Capacitor ($/$\mu$F)	0.05 - 0.09	.07
Service	Nominal Monthly Tariff - India ($)	2-5	2
	Nominal Monthly Tariff - Africa ($)	10-15	10
	Increase in Monthly Tariff (%)	5-50	20
	Increase in Monthly Tariff (%)-Large Loads	30-75	50
	Battery Lifetime (yr)	2-7	5
System	Battery Voltage(V_0)	24	24
	Voltage Lower Limit (V_{tr})	$0.5 - 0.75V_0$	$0.66V_0$
	Solar Panel (W)	50-250	150
	Max Total Power (P/P_0)	0.2-0.5	0.3
	Line Resistance (Ω/km)	0.2	0.2
	Line Time Constant, $\tau = L/R$ (ms)	1-10	1
	Small Load Limit (P/P_0)	0.05-0.08	0.05
	Large Load Limit (P/P_0)	0.12-0.3	0.24

Table 2.2: Interconnected SHS Input Variables

tify stability. Therefore, in simplifying the loading model, the cost related to the capacitor was over estimated, due to the dependence of the capacitor cost on its magnitude. Beyond the simple loading model, businesses, whose need for reliability may be greater than that of a household and who may need to support larger loads, are not explicitly considered. The inclusion of businesses that could face higher tariffs could reduce the projected return on investment.

A key to this technology is that it has the potential to reduce the amount of storage required for off grid systems to run effectively. However, the range of reduction in storage is based on a much larger system of AC, rather than DC, microgrids rather than a system of solar home systems. Therefore, it is possible that this level of reduction is not achievable. There is no analysis in this model that directly calculates the reduction in storage based on any of the system parameters.

Finally, the manner in which the hardware constraints are incorporated neglects the specifics of hardware and converter design. The interconnected systems are assumed identical to the isolated systems with only the addition of a stabilizing capacitor, which could be an oversimplification.

2.6.3 Feasibility Assessment

A network of interconnected solar home systems will only be seen as viable if the associated period for a return on investment is less than that of a collection of isolated systems. Both the technical system parameters and business plan, namely the tarrifs charged for the levels of service and capacity that characterizes each of those level, will alter the ROI. This section will explore the impact *system parameters*. This is not intended to be an exhaustive review but rather to provide intuition for the theory presented in previous sections.

Specifically of interest are the line time constant (τ), the minimum voltage during transients (V_{tr}), and the percent reduction in storage. The total interconnection distance is assumed to be known based on the village layout. The typical distance between households in Indian villages is approximately 19 m [14]. Based on this distance and the assumption that the interconnection structure of the households is not linear

Appliance	Avg Power Consumption (W)
Light	5
Phone Charger	5
Radio	10
Shaver	15
Fan	50
TV	50
Sewing Machine	100

Table 2.3: Power consumption of common appliances

but rather has a sparse but arbitrary structure such that for every 8 households there are 9 interconnections, a total interconnection length of 1.28 kilometers was selected. The remainder of the system parameters and sample business plan components are given in Table 2.2.

Of note is the two different levels of service. The base loading level allows for a household to consume a maximum of 28W while those with a premium service are allowed a maximum of 135 W. The typical consumption of relevant household appliances is given in Table 2.3. The lower level of service easily accommodates phone chargers, lighting and radios. The higher level of service can accommodate productive loads, such as sewing machines, in addition to comfort loads, including TVs and fans.

Table 2.4 gives the the return on investment in months for interconnected solar home systems for a variety of system parameter configurations. There are several important trends to note. First, the ROI trends echo those of the minimum allowable voltage and the time constant of the line. By increasing the minimum allowable voltage and the time constant of the line, a larger capacitor is required for stability. The ROI therefore increases due to the cost of the added capacitance which emphasizes the importance of defining the minimum required capacitance as this work has done. The second relevant trend is that the ROI decreases as the reduction in storage increases. The reduction in storage is possible due to the interconnection structure of the network. Storage is a costly component and therefore its reduction contributes to a decrease in capital costs which in turn lowers the return on investment period.

	Storage Reduction	10%			25%			40%		
	V_{tr}/V_0	0.5	0.66	0.75	0.5	0.66	0.75	0.5	0.66	0.75
τ (ms)	1	18	19	19	18	18	19	17	18	18
	2.5	18	20	20	18	20	20	18	19	20
	5	19	22	23	18	21	22	18	21	22
	10	19	26	27	19	25	27	18	25	26

Table 2.4: ROI (in months) for interconnected solar home systems with various system parameter configurations

In reality, system design would require an analysis of what the attainable reduction in storage is without compromising reliability.

The ROI for identical but isolated solar home systems would be 19 months. By varying the system parameters, it can also be shown that the interconnected systems have the potential to reduce the ROI in comparison to isolated systems. In this analysis, there are a variety of reductions in storage and line time constants that do allow for an improved ROI. However, the minimum voltage level of $0.5V_0$ shows the most consistent potential to reduce the ROI of interconnected systems as compared with isolated systems. This lower bound on voltage may not be acceptable for the loads connected and that must be considered in the system design process. Overall, this analysis demonstrates not only that there is a economic incentive for defining the minimum required capacitance for stable network operation but also that there are parameter configurations such that interconnection of SHS in conjunction with the stability guarantees provides an avenue for reducing the return on investment.

2.7 Conclusion

This chapter examined the instability that arises when a load is added or removed from a DC microgrid where the interconnection structure is unknown. We show that a capacitor of sufficient magnitude placed in parallel with each load serves to stabilize the system. The primary contribution of this work is found in Eqs. (2.29) and (2.20) which, in conjuction with the small signal constraint given in Equation 2.30, dictate the capacitance magnitude for the system to remain stable at each individual load

as a function of the maximum power that load can consume. Two design trade offs were highlighted. First between the power demanded at a load and the capacitance required to guarantee stability. A critical loading level at which the capacitance required is no longer proportional to the loading was discovered and can be utilized to optimize for the system cost without compromising stability. Second, a trade off between the minimum system voltage and the maximum power consumption that can be certified stable at each node.

Several exciting paths needs to be further explored. These include the generalization of the results to certain relevant restricted topologies, more detailed load and source models. Similarly, more research is required to understand how stability can be enforced on secondary control loops on sources [29, 5, 9] in the presence of inductive delays.

Chapter 3

Small-Signal Stability of Systems with Arbitrary Loads: Theory

The ad hoc microgrids described in Chapter 2 represent an accurate but specific model for DC microgrids. Most notably, the model assumed that only constant power loads were used in the network. While this is an accepted approximation for power electronic interfaced loads, a broader variety of loads must be considered in order to broaden the applicability of the analysis. Therefore, this chapter will focus on the small-signal stability of DC microgrids with arbitrary transfer functions, thus making no specific assumptions about the behavior of the load. Recently the problem of stability of CPL based microgrids has attracted substantial attention from the controls community. Beyond what was presented in Chapter 2 and its preceding work, [5], this topic has also been investigated by [24, 26, 29, 4, 10].

We utilize a passivity-based approach to develop a basic stability condition based on the positivity of a quantity we call the Augmented Power Dissipation, which is a linear combination of the real and reactive power of the system. This approach allows for the decomposition of the network into a series of paths for each of the loads, each of which must adhere to the stability criterion developed or for the development of a bound on the network dissipation. We therefore utilize the network structure explicitly in the certification of stability unlike many existing methodologies which only consider the minor loop gain. In this way, our methodology can be applied to

more easily allow the stability constraints to guide network and input filter design.

The layout of this chapter is as follows. First, we will review common methodologies for the stability of DC grids. Next, we will formalize our problem formulation and provide background on power electronics, an important class of load for practical implementation. Then, we will establish the passivity-based stability criterion and show the two different manners in which it can be applied to simplify a network and analyze its stability.

3.1 Traditional Stability Criterion

The power electronics community has traditionally relied on a number of impedance-based stability criterion to evaluate the stability of a DC network. These impedance based criterion are based on bounding the minor loop gain in the complex plane. The minor loop gain, $T_{MLG}(\omega)$, is the ratio of the output impedance, Z_{out}, of one element, typically the network or filter, to the input impedance, Z_{in}, of another, typically a load. More formally, the minor loop gain can be given as

$$T_{MLG}(\omega) = \frac{Z_{out}(\omega)}{Z_{in}(\omega)} \tag{3.1}$$

The minor loop gain directly emerges from the series interconnection of two system with *stable* transfer functions G_1 and G_2. When interconnected the transfer function of the system from the output, $v_{out}(\omega)$, to the input, $v_{in}(\omega)$ is given by

$$\begin{aligned} \frac{v_{out}(\omega)}{v_{in}(\omega)} &= G_1 G_2 \frac{Z_{2,in}}{Z_{2,in} + Z_{1,out}} \\ &= G_1 G_2 \frac{1}{1 + T_{MLG}} \end{aligned} \tag{3.2}$$

The criterion rely heavily on the Nyquist criterion which relates stability to the encirclements of (-1, 0) in the complex plane. Detailed information on this criterion

can be found in [2]. Therefore, each of these criterion develops a sufficient condition for stability by creating forbidden regions in the complex plane which include (-1, 0) to prevent any possible encirclements. However, the manner in which the complex plane is partitioned differ for each method as follows.

Middlebrook

Perhaps the most popular DC stability criterion, the Middlebrook criterion [20] bounds the minor loop gain such that it must remain within the unit circle such that

$$|T_{MLG}(\omega)| < 1 \tag{3.3}$$

For practical design purposes, a safety factor can be included in the form of a gain margin, $GM > 1$. In this formulation, the upper bound on the minor loop gain would be $1/GM$, reducing the radius circle in the complex in which the minor loop gain can exist.

The Middlebrook criterion was originally developed to assess the stability of the interconnection of an input filter with a converter. When the magnitude of the minor loop gain is much less than 1, it can be shown that the dynamics of the converter are not modified. In this manner, the criterion not only provides stability but also consistency which can be beneficial in the context of converter-filter interconnections but can be overly conservative for arbitrary DC grids.

Gain Margin and Phase Margin Criterion

Unlike Middlebrook, the gain margin and phase margin criterion (GMPM) allows for the magnitude of the minor loop gain to be dependent its argument due to the inclusion of a phase margin (PM). The requirement for this criterion can be expressed as: if $|\arg(Z_{out}) - \arg(Z_{in})| > 180° - PM$ then $|T_{MLG}| < 1/GM$ otherwise there is no bound on the minor loop gain. Unlike Middlebrook, this criterion requires knowledge of both magnitude *and* phase.

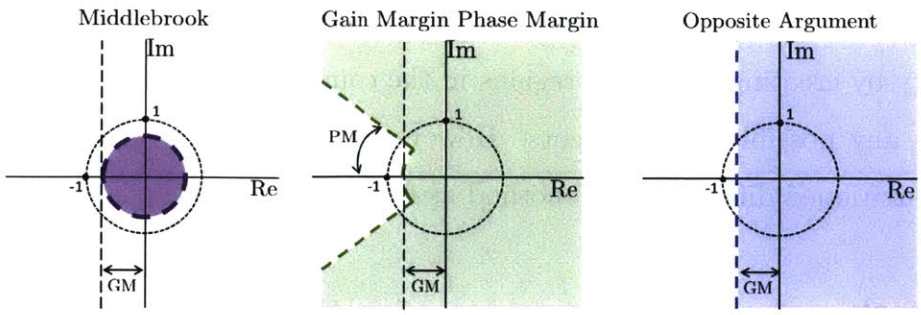

Figure 3-1: Restrictions on the minor loop gain imposed by classical stability criterion

Opposing Argument Criterion

The opposing argument criterion is unlike the previous two criterion presented in that it is more easily defined and conceptualized in rectangular rather than polar coordinates. The oppositing argument criterion partitions the complex plan via a line parallel to the imaginary axis. The resulting bound is that the real part of the minor loop gain is bounded from below by $-1/GM$ such that

$$\mathrm{Re}[T_{MLG}] \leq -\frac{1}{GM} \tag{3.4}$$

Comparison of Criterion

The valid regions for the minor loop gain in the complex plane for the various criterion are given in Figure 3-1. It is of note that both relaxations of the Middlebrook criterion, namely the opposing argument criterion and the gain margin and phase margin criterion, require specific knowledge of both phase and magnitude. This additional knowledge of the load required can cause errors in implementation if the load is not properly modeled and makes the application of the criterion relevant to a single load rather than a class of loads. The following work will strive to rely only on magnitude of the loading, like the Middlebrook criterion. However, unlike Middlebrook, we strive to find a stability criterion that more explicitly utilizes network structure such that the criterion can more easily inform network design.

3.2 Problem Formulation

DC-DC power electronic converters are typically designed to efficiently provide a fairly constant output voltage with control system properly mitigating the input voltage variations. As seen from the network these converters represent a rather complex dynamic behavior, so a dynamic model of the converter needs to be considered for studying the stability of it's operation with the network. A common way to represent a lossless converter is using a single-pole, double-throw (SPDT) switch with a duty cycle D defining the fraction of the cycle spent in position 1. By using lossless elements, the modification of the input voltage is achieved in a manner that can apply to all power throughputs. In steady state, converters can be described by their DC conversion ratio M, the ratio of the output voltage V to the input voltage V_g. This conversion ratio is a function of the duty cycle control input.

To study stability, we utilize a small signal model of the system. Due to the switch, which operates with a frequency on the order of tens of kilohertz, the inductor current and capacitor voltage vary throughout a given cycle with small amplitude around their average values even in steady state. Therefore, to properly account for the low frequency variations, the so-called small-ripple approximation is used where the system is averaged over a period so the switching variations within a given period are neglected. The averaged system can then be linearized about a given operating point to give a small signal model.

While there are several common types of converters, we will focus on the buck converter, given in Figure 3-2a, due to its prevalence. The buck converter, consisting of an inductance L, capacitance C and constant resistance load R, has a conversion ratio $M(D) = D$, such that the converter steps-down the input voltage in proportion to the duty cycle. The small signal model of a buck converter is shown in Figure 3-2b where all uppercase variables refer to the operating point and all lowercase variables refer to the time varying deviations. Since averaging is done over many switching periods, an ideal DC transformer, rather than a switch is used in the small signal model to properly describe dynamics. A formal derivation of this model and

additional background on buck converters are given in [11].

To maintain constant voltage at its output, a converter relies on feedback to modify the duty cycle following any variations in the input voltage. In this work, we consider a buck converter interfaced with a constant resistance on it's output and the control loop to stabilize the output voltage, so that it is seen from the network as a constant power load in steady state. This model is defined in Figure 3-4. To characterize the small signal behavior of the buck converter, we first examine the transfer function from the control input (duty cycle variation) $d(s)$ to the output voltage $v(s)$ which has the following form (detail can be found in [11])

$$G_{vd}(s) = \frac{v(s)}{d(s)} = G_0 \frac{\omega_0^2}{s^2 + 2\zeta\omega_0 s + \omega_0^2} \tag{3.5}$$

with $G_0 = V/D$, $\omega_0 = 1/\sqrt{LC}$ and $\zeta = 1/(2R)\sqrt{L/C}$. In the presence of voltage control, the loop gain of the system is defined as $T = G_{vd}(s)H(s)G_c(s)/V_m$ where H is the sensor gain, $G_c(s)$ is the compensator transfer function and V_m is the voltage of the pulse width modulation. The input admittance transfer function $Y_{\mathcal{L},k}(s)$ can then be defined as

$$Y_{\mathcal{L},k}(s) = \frac{i(s)}{v_g(s)} = \frac{1}{Z_N(s)} \frac{T(s)}{1+T(s)} + \frac{1}{Z_D(s)} \frac{1}{1+T(s)} \tag{3.6}$$

where Z_N is the converter impedance when the output $v(s)$ is nulled and Z_D is the converter impedance in the absence of control input $d(s)$. For a buck converter, these have the following expressions: $Z_N = \frac{-R}{D^2}$ and $Z_D = \frac{R}{D^2} \frac{1+sL/R+s^2LC}{1+sRC}$.

As will be shown in the following sections, much of the analysis relies on the real component of the input admittance. For a buck converter, this quantity is given in Figure 3-3, the corresponding quantities for constant resistance load and a constant power load are given for comparison. A tightly controlled buck converter can be thought of as a constant power load at low frequencies. The buck converter becomes passive at a crossover frequency Ω_C, defined as the frequency above which $\mathrm{Re}[Y_{\mathcal{L}}(\omega)] > 0$. In contrast the constant power load is frequency independent and is never passive. This highlights the need for a more detailed stability analysis than a constant power

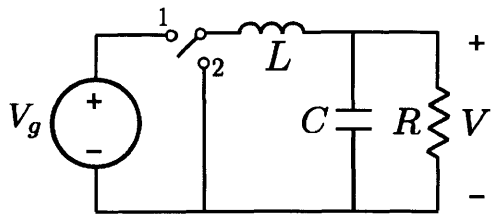

(a) Switching Model

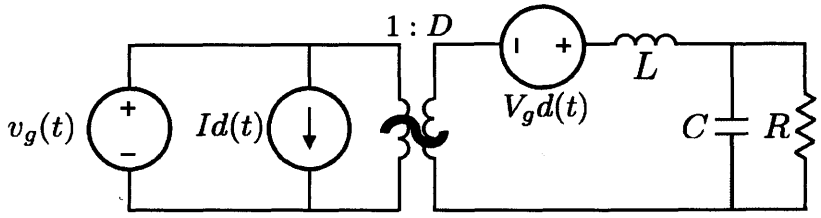

(b) Small signal model

Figure 3-2: Steady state and small signal models of a buck converter

representation can provide for systems with power converters.

In practice, converters are also equipped with an input filter to reject the high-frequency current components from converter switching actions. In this work, the input filter is considered to be part of the network. It is known that improper input filter design can bring instability to an otherwise stable converter, therefore, a careful selection of filter configuration is required. Typically, the whole system is designed to be stable when directly connected to a fixed DC voltage source with the effect of interconnecting line neglected. If the connecting line has substantial impedance, it can interfere with the converter filter and finally lead to instability.

3.3 Effective Load Admittance and Stability Conditions

3.3.1 Effective Admittance Representation

To study small-signal stability of our network we introduce the following vector of node voltage and current perturbations $x_e = [i_e^T . v_e^T]^T$ where both the node current

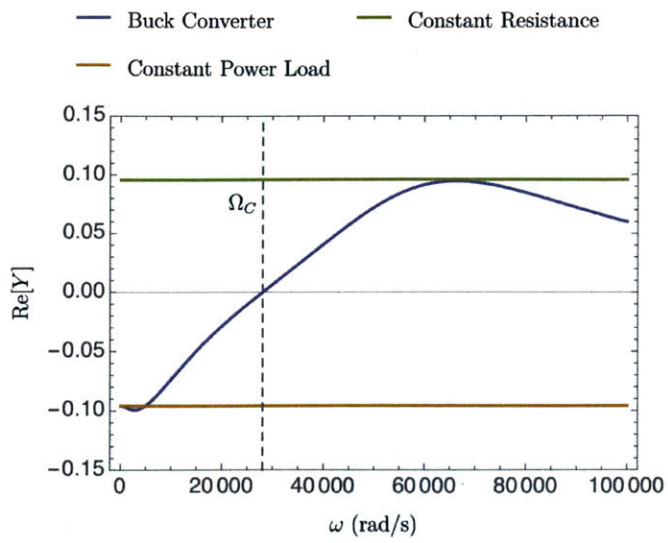

Figure 3-3: Real component of the input admittance transfer functions for a buck converter, constant resistance load and constant power load.

$i \in \mathbb{C}^{|\mathcal{V}|}$ and node voltage $v \in \mathbb{C}^{|\mathcal{V}|}$ being deviations from the equilibrium point, eg. $i_e(t) = I(t) - I_0$.

Next, we define the frequency dependant nodal admittance matrix according to a general rule:

$$i(\omega) = Y(\omega)v(\omega) \tag{3.7}$$

where the full matrix Y includes contribution from network $Y_{\mathcal{N}}$ and loads $Y_{\mathcal{L}}$ with the latter matrix being diagonal. The effective load admittance matrix can be explicitly expressed using converter small-signal model or directly measured.

Our general strategy for proving the stability of the interconnection is based on the well-known "zero exclusion principle" and is closely related to the μ-analysis.

Theorem 4 *The interconnection is stable for any admissible load transfer functions if there exists a quadratic form*

$$W = \mathrm{Re}[v^{\dagger} D(Y_{\mathcal{N}}(\omega) + Y_{\mathcal{L}}(\omega))v] \tag{3.8}$$

that is strictly positive for any harmonic signal $v(\omega) \neq 0$.

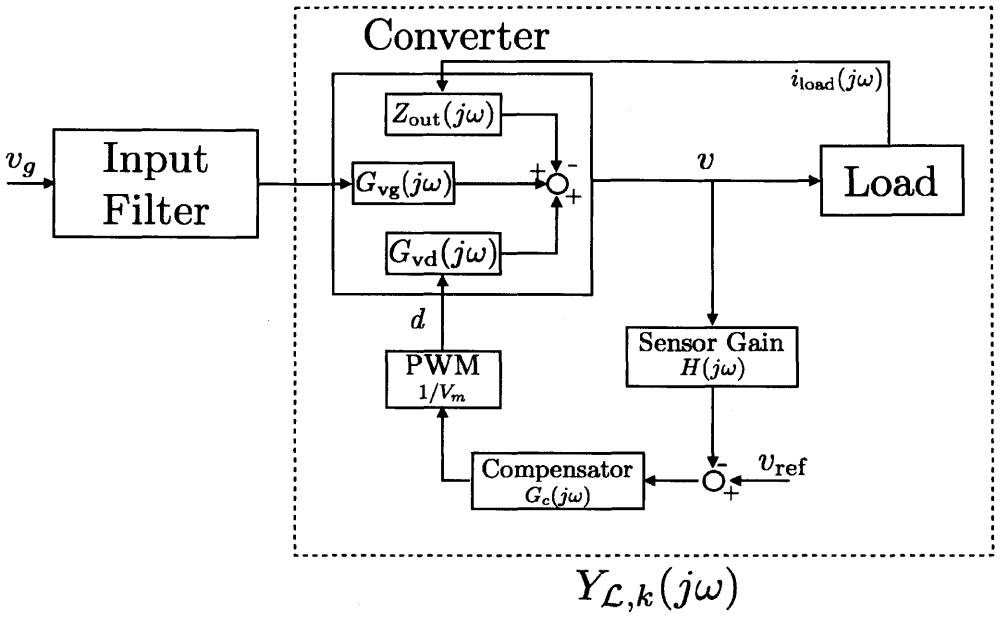

Figure 3-4: Definition of Small Signal Load Model

Proof 9 *This is a well-known principle in the robust control literature. The simple interpretation of the standard proof is the following. Suppose that for some admissible loads there exists a pole in the right hand plane. Consider now a homotopy between the unstable an completely unloaded system (all load admittance are zero $Y_{\mathcal{L}} = 0$). As the unloaded system is stable, there would be a point on a homotopy where the originally unstable pole lies on the imaginary axis at $\omega = \omega_c$. The voltage profile v corresponding to this mode, would then satisfy $(Y_{\mathcal{N}}(\omega_c) + Y_{\mathcal{L}}(\omega_c))v = 0$ and contradict the assumptions of the theorem.*

In the following we consider a specific quadratic functional we refer to as *Augmented Power Dissipation*, that is characterized by $D = \mathrm{e}^{j\phi(\omega)}$. The important property that follows directly from (3.8) is that the total dissipation of the system can be decomposed into the contributions coming from the network $W_{\mathcal{N}} = \mathrm{Re}[v^\dagger D Y_{\mathcal{N}}(\omega)v]$ and loads $W_{\mathcal{L}} = \mathrm{Re}[v^\dagger D Y_{\mathcal{L}}(\omega)v]$ and one can establish the bounds on these components separately. After proving some intermediate results, we derive the sufficient conditions on the network structure that guarantee overall system stability.

Definition 1 *The Augmented Conductance of a two-terminal element with admit-*

tance y_k is defined as

$$G_k(\omega, \phi(\omega)) = \mathrm{Re}[e^{j\phi(\omega)} y_k(\omega)] \tag{3.9}$$

Definition 2 *For a two terminal element characterized by the admittance $y_k(\omega)$ and voltage drop $\nabla_k v(\omega)$, the Augmented Power Dissipation is defined as*

$$W_k = \mathrm{Re}\left[\overline{\nabla_k v} e^{j\phi} y_k \nabla_k v\right] = G_k(\omega) |\nabla_k v|^2 \tag{3.10}$$

The Augmented Power Dissipation coincides with real power dissipation for $\phi = 0$ and with reactive power dissipation for $\phi = \pi/2$. For general $\phi(\omega)$ the corresponding time-domain storage function does not have any well-defined physical meaning. The following results will be useful for constructing the dissipative functionals:

Remark 3 *The Augmented Conductance of resistive-inductive elements with admittance $y = 1/(r + j\omega L)$ is given by*

$$G = \frac{r\cos\phi(\omega) + \omega L \sin\phi(\omega)}{r^2 + \omega^2 L^2} \tag{3.11}$$

The Augmented Conductance is positive whenever $r\cos(\phi(\omega)) + \omega L \sin(\phi(\omega)) > 0$. The biggest value of Augmented Conductance, and thus the highest rate of Augmented Dissipation is achieved for $\tan\phi(\omega) = \omega L/R$ for which $G = 1/\sqrt{r^2 + \omega^2 L^2}$

Remark 4 *For resistive-capacitive elements with $y = 1/(r - j/(\omega C))$ the Augmented Conductance takes the form*

$$G = \omega C \frac{\omega r C \cos\phi(\omega) - \sin\phi(\omega)}{1 + (\omega r C)^2} \tag{3.12}$$

This element remains augmented dissipative whenever $r\omega C \cos(\phi(\omega) - \sin(\phi(\omega)) > 0$

Remark 5 *In the presence of shunt capacitive element with inductive and resistive line with $y = 1/(r + j\omega L) + j\omega C$ the augmented conductance takes the form*

$$G = \frac{r\cos\phi(\omega) + \omega L \sin\phi(\omega)}{r^2 + \omega^2 L^2} - \omega C \sin\phi(\omega) \tag{3.13}$$

A choice of negative ϕ may be required for this element to remain augmented dissipative.

Whenever the overall element admittance magnitude is bounded, the following bound can be established on the absolute value of Augmented Power Dissipation

Lemma 6 *For any two-terminal element k, with bounded magnitude of admittance y_k satisfying $|y_k| \leq Y_k^{\max}$, the absolute value of Augmented Power Dissipation is bounded from above:*

$$\left|\mathrm{Re}\left[\overline{\nabla_k v} e^{j\phi} y_k \nabla_k v\right]\right| \leq Y_k^{\max} |\nabla_k v|^2 \tag{3.14}$$

Proof 10 *Follows directly from* $|\mathrm{Re}[e^{j\phi} y_k]| \leq |e^{j\phi} y_k| = |y_k|$

This observation implies that the constant power load with incrementally negative resistance can inject only some bounded amounts of Augmented Power into the system. Our stability certificates will be based upon matching the Augmented Power injected by the loads with it being dissipated by the network elements

3.3.2 Network Decomposition

In order to derive the stability certificate, we first introduce a path based characterization of the interconnection network.

Definition 3 *A load path $\Pi_k(\omega) = \{e_1, \ldots e_{n_k}\}$ is an ordered set of directed circuit network edges satisfying following properties: i) the end of edge e_m coincides with the beginning of edge e_{m+1} ii) the beginning of the edge e_1 coincides with the load $k \in \mathcal{L}$, iii) no edge appears twice in the path, iv) the end of the last edge e_{n_k} does not coincide with the origin and is denoted as $\mathrm{end}(\Pi_k)$, and v) the augmented conductance G_e of every element $e \in \Pi_k$ along the path is positive: $G_e > 0$.*

Note, that explicit dependence of the path $\Pi_k(\omega)$ on the frequency emphasizes that different paths can be used for different frequencies. For every path we define the aggregate Augmented Conductance:

Definition 4 *The aggregate Augmented Conductance G_{Π_k} of the path Π_k is related to the conductance of individual elements via the following series interconnection relation:*

$$\frac{1}{G_{\Pi_k}} = \sum_{e \in \Pi_k} \frac{1}{G_e} \tag{3.15}$$

This definition appears naturally in the following bound on the Augmented Power Dissipation:

Lemma 7 *If the network is composed of elements with positive Augmented Conductances $G_k > 0$, the aggregate Augmented Power Dissipation $W_{\Pi_k} = \sum_{e \in \Pi_k} W_e$ of all elements $e \in \Pi_k$ along the path is bounded from below by*

$$W_{\Pi_k} \geq G_{\Pi_k} \left| v_k - v_{\mathrm{end}(\Pi_k)} \right|^2 \tag{3.16}$$

Proof 11 *Define $\pi_e = G_{\Pi_k}/G_e > 0$, so that $\sum_{e \in \Pi_k} \pi_e = 1$ in accordance to* (3.15). *In this case one has*

$$\begin{aligned} W_{\Pi_k} &= \frac{1}{G_{\Pi_k}} \sum_{e \in \Pi_k} \pi_e \left| G_e \nabla_e v \right|^2 \\ &\geq \frac{1}{G_{\Pi_k}} \left| \sum_{e \in \Pi_k} \pi_e G_e \nabla_e v \right|^2 \\ &= G_{\Pi_k} \left| v_k - v_{\mathrm{end}(\Pi_k)} \right|^2 \end{aligned} \tag{3.17}$$

Here we have used the Jensen's inequality and the definition of the path.

Definition 5 *A load path decomposition of the network is a set of load paths Π_k assigned for every load $k \in \mathcal{L}$, such that there is only one path passing through every two-terminal element $k \in \mathcal{E}$.*

Note, that the load path decomposition may not exist for original circuit, for example there is only a single source and multiple loads connected to it through a single line. However, the path decomposition can be constructed for an equivalent electric circuit where some individual network elements are represented as a parallel interconnection of multiple ones, like illustrate on Figure 3-5 . In the following,

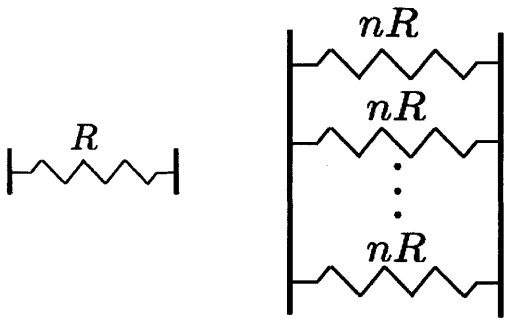

(a) (b)

Figure 3-5: The example decomposition of a two port resistive element to allow for n paths.

we assume that the network circuit has been transformed to allow for load path decomposition. Then, the following lemma establishes the ground for the central result of the paper:

Lemma 8 *The total Augmented Power $W_{\mathcal{N}}$ dissipated in the network characterized by the path decomposition Π_k with $k \in \mathcal{L}$ is bounded from below by the following expression:*

$$W_{\mathcal{N}} \geq \sum_k G_{\Pi_k} \left| v_k - v_{\mathrm{end}(\Pi_k)} \right|^2 \tag{3.18}$$

Proof 12 *Given that there is at most one path passing through every element, one has $W_{\mathcal{N}} \geq \sum_{k \in \mathcal{L}} W_{\Pi_k}$. Then the relation* (3.18) *follows immediately from Lemma 7.*

This allows us to finally formulate the following central result of the work:

Theorem 5 *Consider a network composed of elements with positive Augmented Conductances and constant voltage sources with $v_k = 0$. Assume that for every ω, there exists a path decomposition $\Pi_k(\omega)$ such that every path ends either at the ground or source nodes, i.e. $v_{\mathrm{end}(\Pi_k)} = 0$. Then, the total Augmented Power Dissipation in the system $W_{\mathcal{N}} + W_{\mathcal{L}}$ is positive for any non-zero voltage signal whenever for every $k \in \mathcal{L}$ one has $G_{\Pi_k}(\omega) > Y_k^{\max}(\omega)$.*

Proof 13 *In accordance to lemmas 6 and 8, the total Augmented Power Dissipation*

of the system can be decomposed as

$$W_{\mathcal{N}} + W_{\mathcal{L}} \geq \sum_{k\in\mathcal{L}} W_{\Pi_k} - y_k|v_k|^2$$
$$\geq \sum_{k\in\mathcal{L}} |v_k|^2 \left(G_{\Pi_k} - Y_k^{\max}\right) > 0. \tag{3.19}$$

3.3.3 Upper Bound on Dissipation

In this section we establish the upper bounds on the augmented dissipation for an alternative to the decomposition of a network into paths. The objective is to derive an alternative approach to defining the worst-case configuration in the absence of the path decomposition requirement that each individual element remains passive.

We denote the augmented admittance by $Y = G \pm jB$ with symmetric positive definite G, B with sign in Y dependent on the augmentation angle. Similarly, the inverse is given by $Y^{-1} = R \mp jX$. Here we consider a system composed of load nodes denoted by set $\mathcal{L}$ and internal nodes denoted by I. The load nodes are typically connected to the internal nodes via some type of filter. With power electronic loads, this filter would reduce the effects of harmonics.

Theorem 6 *Given a system satisfying $G_{I\mathcal{L}} = \beta(\omega)B_{I\mathcal{L}}$ with $\beta(\omega) > 1$, the total dissipation can bounded from above such that*

$$Re[v^t Y v] \leq v_{\mathcal{L}}^t G_{\mathcal{L}\mathcal{L}} v_{\mathcal{L}} \tag{3.20}$$

where $\mathcal{L}$ denotes the subset of nodes that are loads.

Proof 14 *The voltage values on internal buses satisfy $Y_{I\mathcal{L}}v_{\mathcal{L}} + Y_{II}v_I = 0$, hence the total dissipation is given by*

$$\begin{aligned}
\mathrm{Re}\left[v^t Y v\right] &= \mathrm{Re}\left[v_{\mathcal{L}}^t \left(Y_{\mathcal{L}\mathcal{L}} - Y_{\mathcal{L}I}Y_{II}^{-1}Y_{I\mathcal{L}}\right) v_{\mathcal{L}}\right] \\
&= v_{\mathcal{L}}^t \left[G_{\mathcal{L}\mathcal{L}} - (G_{\mathcal{L}I} \pm jB_{\mathcal{L}I})(R_{II} \mp jX_{II})(G_{I\mathcal{L}} \pm jB_{I\mathcal{L}})\right] v_{\mathcal{L}} \\
&= v_{\mathcal{L}}^t G_{\mathcal{L}\mathcal{L}} v_{\mathcal{L}} - v_{\mathcal{L}}^t \left[G_{\mathcal{L}I}R_{II}G_{I\mathcal{L}} - B_{\mathcal{L}I}R_{II}B_{I\mathcal{L}} + 2G_{\mathcal{L}I}X_{II}B_{I\mathcal{L}}\right] v_{\mathcal{L}}
\end{aligned} \tag{3.21}$$

The second term of 3.21 is can be shown to be negative under certain conditions. This term has three contributions. The first and third contributions are positive by definition. We assume that the filter admittance has the form $Y_{I\mathcal{L}} = G_{I\mathcal{L}} \pm jB_{I\mathcal{L}}$ *where* $G_{I\mathcal{L}} = \beta(\omega)B_{I\mathcal{L}}$. *The second contribution can then be shown to take the quadratic form of*

$$(B_{I\mathcal{L}}v_{\mathcal{L}})^t\left[\beta(\omega)^2 R_{II} - R_{II} + 2\beta(\omega)X_{II}\right](B_{I\mathcal{L}}v_{\mathcal{L}}) \tag{3.22}$$

which is positive definite when $\beta(\omega) > 1$. *The dissipation can thus be bounded from above.*

Remark 6 *The condition* $G_{I\mathcal{L}} = \beta(\omega)B_{I\mathcal{L}}$ *can be enforced by moving the boundary that separates the load filters from the network. For example, if for a given load filter* $G < B$, *then transferring a part of augmented inductance* B *to the network allows one to satisfy the criterion.*

Remark 7 *Of special interest is augmentation by* $\phi = \pi/2$ *that transforms capacitive elements into resistive ones. For this augmentation, the* LR *elements are characterized by* $Y = (\omega L - jR)/(\omega^2 L^2 + R^2)$.

Next, we assume that each load has a series filter with inductance L *and we assume that all the corresponding resistance is moved to the network. In this case* $B_{LI} = 0$ *and the upperbound is valid for all frequencies. The total augmented dissipation on the load is upper-bounded by* $v^2/(\omega L)$. *Hence, the stability condition is given by*

$$\omega C - \frac{1}{\omega L} > Y^{\max}(\omega) \tag{3.23}$$

3.4 Conclusion

This chapter has presented a novel method for certifying the stability of a DC network with loads represented by generic transfer functions via an Augmented Power Dissipation criterion. While our approach is conceptually similar to the traditional Middlebrook and other similar criteria, it's unique in its ability to capture the effects of network topology. We interpret the criterion presented in two manners: first,

via a path decomposition of the network and second, via bounding the augmented dissipation. This chapter has laid the theoretical foundation for a new method to certify network stability. The next chapter will explore practical implementations, limitations and benefits of this criterion.

Chapter 4

Small-Signal Stability of Systems with Arbitrary Loading: Application

The previous chapter introduced the concepts of Augmented Power Dissipation and Augmented Conductance which can provide network-aware stability certificates for DC grids. The goal of this chapter is to provide insight into the utilization of these certificates. We begin by returning to a simple two bus system and understanding the implications of various augmentations. We use this example to relate the derived criterion to the canonical Middlebrook criteria. Next we present a number of examples developed to show the implementation of the stability certificates.

4.1 Augmented Power Dissipation Stability Analysis of a 2 Bus System

Just as in Chapter 2, a two-bus system can be meaningful and illustrative example to show the application of a stability criterion. However, unlike in Chapter 2, we will consider an arbitrary load rather than a constant power load to preserve the generality of the analysis. We will define some arbitrary load at bus 2 with impedance and admittance as follows

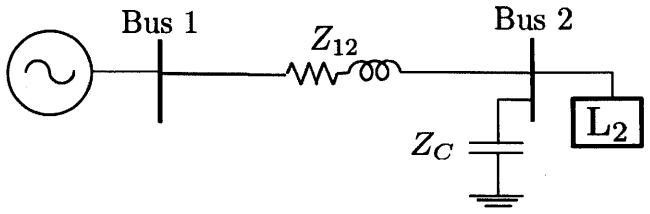

Figure 4-1: Annotated 2 bus system

$$Z_{L2} = R_{L2}(\omega) + jX_{L2}(\omega) \tag{4.1}$$

$$\begin{aligned} Y_{L2} &= Z_{L2}^{-1} \\ &= \frac{R_{L2}(\omega) - jX_{L2}(\omega)}{|Z_{L2}|^2} \end{aligned} \tag{4.2}$$

The lines are considered to be resistive and inductive with admittance $Y_{12} = 1/Z_{12} = (R_{12} - j\omega L_{12})/|Z_12|^2$ where $Z_{12} = R_{12} + j\omega L_{12}$. A capacitor is placed in parallel with the load and has admittance $Y_C = 1/Z_C = j\omega C$. This system is given in Figure 4-1.

We can define the network matrix $\mathcal{Y}_N(\omega)$ and the load matrix $\mathcal{Y}_\mathcal{L}(\omega)$ as

$$\mathcal{Y}_N(\omega) = \begin{bmatrix} Y_{12}(\omega) & -Y_{12}(\omega) \\ -Y_{12}(\omega) & Y_{12}(\omega) + Y_C(\omega) \end{bmatrix} \tag{4.3}$$

and

$$\mathcal{Y}_\mathcal{L}(\omega) = \begin{bmatrix} 0 & 0 \\ 0 & Y_{L2}(\omega) \end{bmatrix} \tag{4.4}$$

Then, in accordance with Theorem 4, the augmented dissipation can be defined as

$$W = \mathrm{Re}[e^{j\phi}(Y_{12}(\omega) + Y_C(\omega) + Y_{L2}(\omega))]|v_2|^2 \tag{4.5}$$

Therefore to prove stability it is necessary to show that

$$Re[e^{j\phi}(Y_{12}(\omega) + Y_C(\omega) + \alpha Y_{L2}(\omega))] > 0 \tag{4.6}$$

for all frequencies ω and $\alpha \in [0, 1]$ where α has been introduced to make explicit the dependence of the derivation on a homotopy drawn between a loaded and unloaded system.

4.1.1 Admittance Interpretation of Zero Crossing

In a two bus system, there are no restrictions on $\phi(\omega)$ implying that augmentation angle can be chosen to align total system admittance vector with the positive real axis such that

$$\max_{\phi(\omega)} \text{Re}[e^{j\phi}(Y_{12}(\omega) + Y_2(\omega) + \alpha Y_{L2}(\omega))] = |Y_{\mathcal{N}}(\omega) + \alpha Y_{L2}(\omega)| \geq 0 \tag{4.7}$$

By relating the augmented dissipation of the network to the magnitude of the total dissipation, it is clear that the only condition in which Theorem 4 will not hold is when the dissipation of the network is exactly balanced by that of the scaled load resulting in no overall dissipation. This case can only occur when the admittance vectors are **co-linear**. Therefore, the system will be unstable if there exists $\alpha \in [0, 1]$ such that

$$Y_{\mathcal{N}}(\omega) + \alpha Y_{\mathcal{L}}(\omega) = 0 \tag{4.8}$$

or equivalently

$$\frac{|Y_{\mathcal{N}}(\omega)|}{|Y_{\mathcal{L}}(\omega)|} > 1 \tag{4.9}$$

given $\angle Y_{\mathcal{N}}(\omega) = \angle Y_{\mathcal{L}}(\omega) + \pi$ and $\omega < \omega_c$ where ω_c is the crossover frequency of the load. It is of note that this connection relies on knowledge of both the magnitude and phase of the network and load admittances while Middlebrook relies solely on magnitude. This example was provided because it allows for the ability to connect the notion of the zero-crossing on which Theorem 4 is based with the admittance

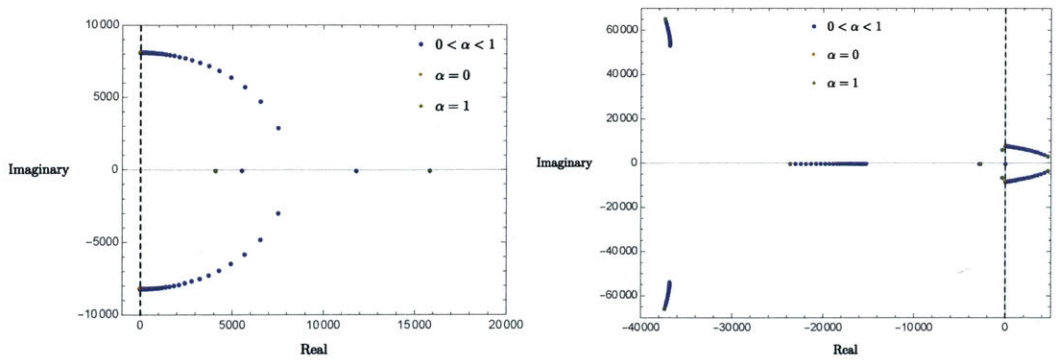

(a) Constant Power Load

(b) Buck Converter

Figure 4-2: The movement of the zeros of the admittance transfer function of a two bus system with a capacitor placed in parallel to the given load.

vectors. Namely, the α such that the network and scaled load admittances directly cancel is the same alpha that brings the zeros of the admittance transfer function to the imaginary axis. An illustration of the homotopy for a constant power load and a buck converter is given in Figure 4-2. It is of note that, when the system is completely unloaded, the zeros are finite due to the presence of the parallel load capacitor. In the absence of the capacitor, a system of just a resistive and inductive line will have the zeros of its admittance transfer function at infinity. This can easily be shown by verifying the limit of $Y_{12}(\omega)$ as $\omega \to \infty$ is 0. Conversely, the limit of $Y_{12}(\omega) + Y_C(\omega)$ as $\omega \to \infty$ is finite and therefore ∞ is not a zero of the network admittance function. The theorem upon which Theorem 4 is based relies on finite zeros at the start of the homotopy. For this reason, a capacitor in the system is critical to the proper utilization of Theorem 4.

4.1.2 Implication of Augmentation Angle $\phi(\omega)$

As exploited in the previous section, there are no bounds on the augmentation angle due of a two bus system when considered in full. However, this system does provide a useful lens to observe the implications of different augmentation angle, which may be required for the dissipation bounding or path decomposition methodologies.

As a point of comparison, we introduce the Middlebrook criterion for this same two bus system. According to Middlebrook, the ratio of the network impedance to

that of the load impedance, known as the minor loop gain, must remain less than 1. The network in this situation is comprised of the resistive inductive line in parallel with the capacitor. Therefore the criterion can be expressed as follows:

$$\begin{aligned} \frac{|Z_N|}{|Z_{L2}|} &< 1 \\ \frac{|(Z_{12} \parallel Z_C)|}{|Z_{L2}|} &< 1 \\ \frac{1}{|Z_{L2}|} = |Y_{L2}| &< \sqrt{\frac{1 - 2CL\omega^2}{|Z_{12}(\omega)|^2} + C^2\omega^2} \end{aligned} \tag{4.10}$$

The final formulation places an upper limit on the magnitude of the load impedance. Importantly, this formulation will allow for easy comparison between Middlebrook and the Augmented Dissipation methods across varying values of $\phi(\omega)$.

Four cases of augmentation will be considered: no augmentation to allow for paths through only lines, augmentation to allow for paths through only shunt capacitors, augmentation to maximize the dissipation of the line and augmentation to maximize the dissipation of the capacitor. These admittance vector representations of these augmentations are given in Figure 4-3

Path via Resistive-Inductive Line $\phi(\omega) = 0$

In the network decomposition method paths can be drawn from the load to a source or two the ground. Two common paths are through a series of inductive-resistive lines and through a capacitor. The path decomposition requires that each two-terminal element remain dissipative. Here we consider the path through the line. This path does not require augmentation. A positive augmentation to increase dissipation in the line will make the capacitor non dissipative. A negative augmentation will reduce the dissipation of the line and increase the dissipation of the capacitor such that the path is no longer purely from the load to the source. Therefore, at $\phi = 0$, with no augmentation, all dissipation comes from the line corresponding to a path from the

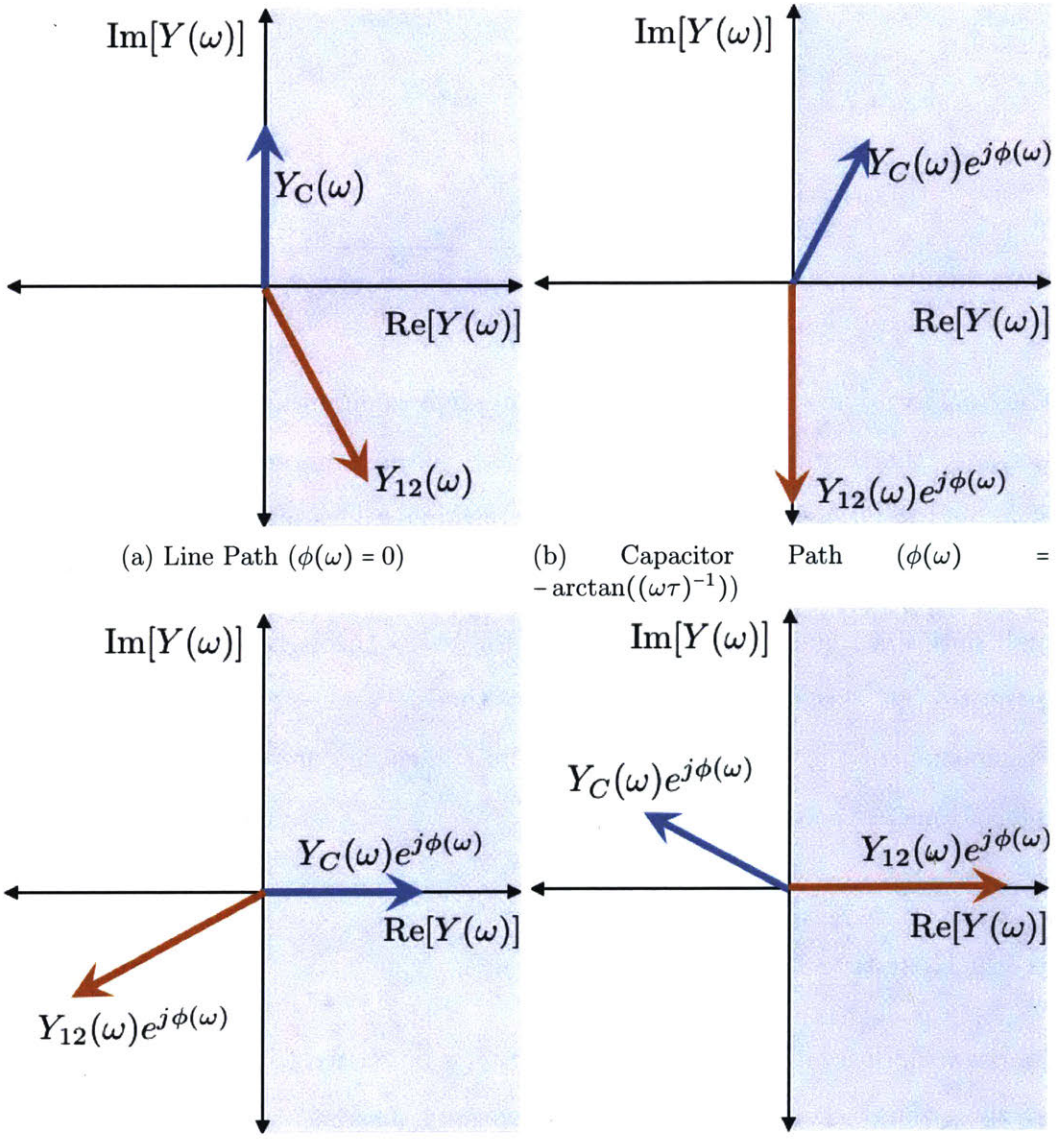

(a) Line Path ($\phi(\omega) = 0$)

(b) Capacitor Path ($\phi(\omega) = -\arctan((\omega\tau)^{-1})$)

(c) Maximum Line Dissipation ($\phi(\omega) = \arctan(\omega\tau)$)

(d) Maximum Capacitor Dissipation ($\phi(\omega) = -\pi/2$)

Figure 4-3: Admittance vector representation of augmentation by various $\phi(\omega)$ for a two bus system

load to the source. The constraints on this system can be characterized as follows:

$$\begin{aligned} \mathrm{Re}[Y_{12} + j\omega C + Y_{L2}] &> 0 \\ \mathrm{Re}[Y_{12}] - |Y_{L2}|_{\max} &> 0 \\ \frac{R_{12}}{|Z_{12}(\omega)|^2} &> |Y_{L2}|_{\max} \end{aligned} \tag{4.11}$$

It is important to note that because the capacitor does not enter into the system without augmentation such that the path only goes through the resistive-inductive lines, these constraints are equivalent to a two bus system without a capacitor for high frequency stabilization.

At low frequencies, the upper bound on the magnitude of the load admittance is $1/R_{12}$. However, at high frequencies, the upperbound approaches 0 so no loading can be supported. This intuitively demonstrates the role of the capacitor in stability. When the capacitor is not utilized, as is the case with no augmentation since the admittance of a capacitor is purely imaginary, no loading can be supported at high frequencies. However, even in the absence of augmentation, an acceptable bound on load admittance can be found at low frequencies to stabilize the load. The bound presented here echoes Middlebrook as the frequency approaches 0.

Path via Capacitive Element $\phi(\omega) = -\arctan((\omega\tau)^{-1})$

Given the importance of the capacitor for stabilization at high frequencies, it is necessary to consider a path through the capacitor. This can most easily be seen through a frequency-dependent rotation that aligns the line admittance vector with the negative imaginary axis. This augmentation corresponds to the capacitor being the only dissipative element. The rotation $\phi(\omega) = -\tan^{-1}((\omega\tau)^{-1})$ aligns the line admittance

vector with the imaginary axis such that

$$\begin{aligned} \mathrm{Re}[e^{-j\arctan(1/\omega\tau)}(Y_{12} + j\omega C + Y_{L2})] &> 0 \\ \omega C \sin(\arctan(1/\omega\tau)) - |Y_{L2}|_{\max} &> 0 \\ \frac{\omega C R_{12}}{|Z_{12}(\omega)|} &> |Y_{L2}|_{\max} \end{aligned} \tag{4.12}$$

At high frequencies, the upper bound on the magnitude of the load admittance approaches CR_{12}/L_{12} even as the admittance of the capacitive element scales with frequency. To keep both elements passive, the augmentation angle is limited. Therefore, as the frequency grows, the augmentation angle decreases such that only a small fraction of the capacitor's admittance can be utilized for stabilization.

Maximal Line Dissipation $\phi(\omega) = \arctan(\omega\tau)$

The past two selections of $\phi(\omega)$ have guaranteed that all two terminal elements, namely the capacitor and the line, remain passive under the augmentation as is required for the network decomposition. However, it is also important to understand the implication of relaxing this constraint. Thus, if a positive $\phi(\omega) = \arctan(\omega\tau)$ is chosen to maximize the augmented dissipation of the line element, the capacitive element can be regarded as a load such that

$$\begin{aligned} \mathrm{Re}[e^{j\arctan(\omega\tau)}(Y_{12} + j\omega C + Y_{L2})] &> 0 \\ |Y_{12}| - \omega C \sin(\arctan(\omega\tau)) - |Y_{L2}|_{\max} &> 0 \\ \frac{1 - \omega^2 C L_{12}}{|Z_{12}(\omega)|} &> |Y_{L2}|_{\max} \end{aligned} \tag{4.13}$$

Such an augmentation can be beneficial as at low frequencies the dissipation of the line is large in comparison to that of the capacitor. In this formulation, the capacitor will act as a small load while the total augmented dissipation of the line increases substantially due to its alignment with the real axis.

Maximal Capacitor Dissipation $\phi = -\pi/2$

Conversely, at high frequencies, the admittance vector from the capacitor would be much larger than that of the line. In this case, maximization of the dissipation due to the alignment of the capacitor admittance vector with the positive real axis would cause the line would become non passive and act as a load. As such the resulting condition for stability would imply that

$$\begin{aligned} \mathrm{Re}[e^{-j\frac{\pi}{2}}(Y_{12} + j\omega C + Y_{L2})] &> 0 \\ \mathrm{Re}[-jY_{12}] + \omega C - |Y_{L2}|_{\max} &> 0 \\ \omega C - \frac{\omega L_{12}}{|Z_{12}|^2} &> |Y_{L2}|_{\max} \end{aligned} \tag{4.14}$$

At high frequencies, this condition approaches $\omega C - 1/\omega L$. This echoes the upper bound on dissipation bound in 3.23. Unlike the high frequency bound found via a path through the capacitor, this bound is frequency dependent and allows for larger load admittances at high frequencies.

Summary

A summary on the bounds of the magnitude of the line impedance to that of the load impedance can be found in Table 4.1. This exercise provides insight into the role of the network and specific elements in the stabilization of loads. At low frequencies, the network acts as a passive element that aids in the stabilization of the load. However, at high frequencies, the network becomes an active element that must then be stabilized by the capacitors.

4.1.3 Relationship to Middlebrook Criterion

The form of Middlebrook can easily be recovered from the path decomposition interpretation of the *Augmented Dissipation* Criterion. For a network path of arbitrary impedance, $Z_{\Pi_k}(\omega) = R(\omega) + jX(\omega)$, the corresponding conductance can be written as

Method	Upperbound on $\lvert Y_{L2}\rvert$
Middlebrook	$\sqrt{\frac{1-2CL_{12}\omega^2}{\lvert Z_{12}(\omega)\rvert^2} + C^2\omega^2}$
Aug. Dissip. ($\phi(\omega) = 0$) Line Path	$\frac{R_{12}}{\lvert Z_{12}(\omega)\rvert^2}$
Aug. Dissip. ($\phi(\omega) = -\arctan(1/\omega\tau)$) Capacitive Path	$\frac{\omega C R_{12}}{\lvert Z_{12}(\omega)\rvert}$
Aug. Dissip.($\phi(\omega) = \arctan(\omega\tau)$) Maximizing Line Contribution	$\frac{1-\omega^2 CL_{12}}{\lvert Z_{12}(\omega)\rvert}$
Aug. Dissip. ($\phi(\omega) = -\pi/2$) Maximizing Cap. Contribution	$\omega C - \frac{\omega L_{12}}{\lvert Z_{12}\rvert^2}$

Table 4.1: Stability constraints for 2 bus system with capacitor parallel to load

$$G_{\Pi_k}(\phi(\omega)) = \frac{R(\omega)\cos(\phi(\omega)) + X(\omega)\sin(\phi(\omega))}{|Z_{\Pi_k}|^2}. \tag{4.15}$$

Let us now optimize this conductance with and augmentation angle $\phi_{\text{opt}} = \arctan(X/R)$. A rotation by ϕ_{opt} aligns the admittance vector with the real axis. The Augmented Conductance then is simply the magnitude of the admittance given an optimal rotation. We note, that due to the restriction that all elements in the network should remain passive, the optimal rotation can sometimes be not allowable due to the requirement of the decomposition that individual elements remain passive. After any non-optimal rotation, the resulting Augmented Conductance is the projection of this rotated vector onto the real axis and can be expressed as

$$G_{\Pi_k}(\phi_{max}(\omega)) = \eta(\phi_{max}(\omega), \omega)|Y| \tag{4.16}$$

where $\eta(\phi(\omega), \omega)$ is an attenuation factor easily derived from equation (4.15), varying between 0 and 1, due to the restrictions the passivity requirements impose on the angle $\phi(\omega)$ which may prohibit the optimal rotation. If the optimal rotation is admissible, the attenuation factor is 1. This formulation of the Augmented Conductance allows for Theorem 5 to be expressed as

$$\frac{|Z_{\mathcal{L}}|}{|Z_{\Pi_k}|} > \eta^{-1}(\phi(\omega), \omega) \tag{4.17}$$

This echoes the form of the Middlebrook criterion. A notable difference is that the impedance ratio must be greater than or equal to 1. The bounds proposed here approach Middlebrook when the augmentation angle is close to or at the optimal angle.

This representation provides some intuition for not relying on the path decomposition at high frequencies. At high frequencies the allowable augmentation angle is much smaller than the optimal augmentation angle for the capacitive element. Therefore relying on bounding the dissipation is more prudent and harnesses more of the dissipation of the capacitor.

This distinction can more clearly be seen in Figure 4-4 which gives a comparison of the bounds for a two bus system that were presented in Table 4.1. For simplicity the system parameters of R, L, and C were all set to 1. It can be seen that at high frequencies, the utilization of the capacitive path results in a much smaller lower bound on load admittance than when the capacitor dissipation is maximized with an augmentation of $-\pi/2$. Further, at high frequencies, the bound given by an augmentation of $-\pi/2$ approaches that of Middlebrook. At low frequencies, the bounds from both the utilization of the line path and the maximization of the line dissipation similarly approach Middlebrook.

Overall, the utilization of path decomposition and no augmentation at low frequencies and the maximization of the capacitive dissipation at high frequencies provide upper bounds for the load admittance that mirror those of Middlebrook. Therefore, this methodology can provide comparable stability guidelines to the canonicald Middlebrook and, in more complex systems, be explicitly aware of network structure.

4.1.4 General Network Stability Guidelines

In order to apply the certificates to actual networks appearing in a microgrid context, we define simple criteria that guarantee existence of paths with sufficiently high Augmented Conductance to support a given load below its crossover frequency Ω_c. In accordance to (3.15), the path has a high conductance only if all of its elements are conductive enough. On the other hand, as discussed in remarks 3 and 4, the Aug-

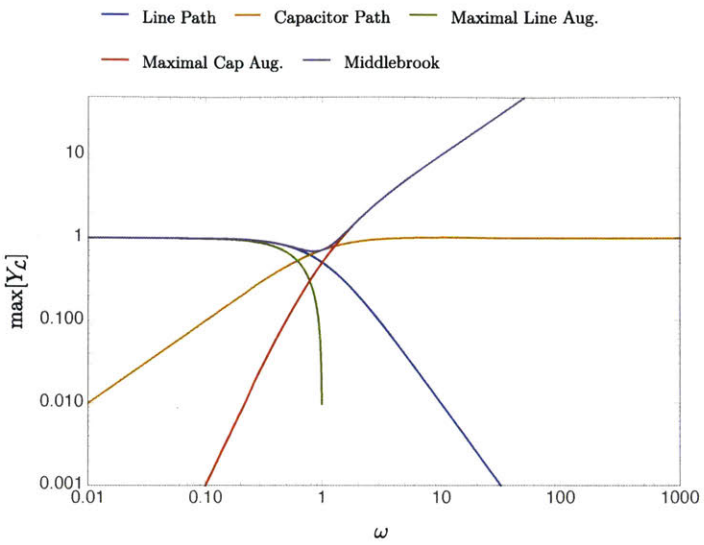

Figure 4-4: A comparison of the upper bounds on $Y_\mathcal{L}$

mented Conductance of inductive elements decreases at high frequencies, and paths with only inductive elements cannot be used to certify stability at high frequencies. At the same time, the Augmented Conductance of capacitive elements goes to zero at small frequencies and grows at high frequencies, and can be naturally used to certify the stability there. Hence, we conclude that if the load is not passive at high frequencies, namely that real part of load admittance remains negative, at least two kinds of paths need to be utilized to certify the overall stability of the system.

In real microgrids, inductive lines are commonly used to interconnect the loads with sources. The common assumption employed in previous studies on the subject is that the time-constant of inductive elements is bounded from above: $L_k/r_k < \tau_L$. This time constant is usually determined by the kind of wires used for interconnection. Both the inductance L_k and resistance r_k scale linearly with the length of the wire, so the time-constant depends only on the type of wires. Assume that there is an equivalent circuit allowing a proper load path decomposition such that for a given load k there is an inductive path Π_k to the source, and the resistance of the elements along the path is given by r_e with $e \in \Pi_k$. Then, the conductance of individual element is bounded from below by $G_e > 1/(r_e + r_e\omega^2\tau_L^2)$. While for the total conductance for

a non-augmented ($\phi(\omega) = 0$) power is given by

$$G_{\Pi_k} = \frac{1}{R_{\Pi_k}} \frac{1}{1 + (\omega\tau_L)^2}, \tag{4.18}$$

where $R_{\Pi_k} = \sum_{e \in \Pi_k} r_e$ is the total resistance of the path Π_k. For a constant $Y_k^{\max}$, independent of ω, this path certifies stability in the band of frequencies $|\omega| < \Omega_k^L$ with

$$\Omega_k^L = \frac{1}{\tau_L} \sqrt{\frac{1}{R_{\Pi_k} Y_k^{\max}} - 1}. \tag{4.19}$$

If rather than using the upper bound, there is an explicit dependence of the admittance magnitude on ω the corresponding frequency band is determined by the solutions of inequality $G_{\Pi_k}(\omega) > |y_k(\omega)|$. Note that augmentation with some positive angle $\phi(\omega)$, as was demonstrated in Section 4.1.2, could improve the bandwidth; however such augmentation will rotate the admittance of a capacitive element into the left half plane so that its real part becomes negative. Therefore, the capacitive elements will inject Augmented Power which compromises the assumption of the Theorem 5 where all the network elements, even those not participating in path decomposition, are required to have positive Augmented Conductance under any admissible rotation. This issue can be dealt with by constructing additional paths to balance the capacitors Augmented Power injection, however this is beyond the scope of the current work where we will only consider the non-augmented inductive paths.

Next, we proceed to certification of stability for high frequency region. Certification for high frequencies can be achieved through the use of a path through a capacitive element or through development of an upper bound on dissipation via parallel load capacitors. Each of the two methods has different situations for which it is best suited. The use of a path through a capacitive element does not require that a capacitor be placed parallel to the load. The capacitor can be placed throughout the network and a path can be drawn through an inductive-resistive line and the capacitor to ground. However, the magnitude and crossover frequency of the load is critical in the ability to separate the load and capacitor as admittance the inductive-resistive

line will diminish the ability of the path to support the load at higher frequencies. A relevant example will be presented in Section 4.2.1. In practice, due to residual capacitance at each load, the assumption of a capacitor at each load is not limiting and therefore an upper bound on capacitance can be used. The upper bound on capacitance does not rely on the passivity of individual elements and therefore can exploit the full dissipation of the capacitive element, via an augmentation by $-\pi/2$, rather than only making use of a fraction of the augmentation. Further, some loads require a parallel load capacitor. If we assume that the bound on load admittance stays constant for all the frequency range - a CPL assumption, than the only way to certify stability is to place capacitor directly at the load bus. Given the decay of inductive conductance with frequency according to (3.11), any path certifying the stability can not go through any of inductive elements.

For the development of general stability guidelines, uniformity in network construction and independence of constraints were prioritized such that a capacitor is considered to be placed at each load. As such we can exploit the upper bound on dissipation given in Equation 3.23 to find the frequency band $|\omega| > \Omega_k^C$ for which the capacitor stabilizes the load with

$$\Omega_k^C = \frac{Y_k^{\max} + \sqrt{(Y_k^{\max})^2 + 4C/L}}{2C} \tag{4.20}$$

In isolation, each load can certified to be stable only if the two frequency bands given by inductive paths - equation (4.19), and upper bound on dissipation - equation (4.20) - overlap, i.e. $\Omega_k^C < \Omega_k^L$. These frequency bands allow for the choice of three free parameters: the path resistance R_{Π_k}, the parallel load capacitance C_k, and the input filter inductance L_k. These parameters can thus be optimized to find the maximum load admittance that can be supported.

When a system contains multiple loads, the overlap of frequency bands must themselves overlap. This requirement ensures that when augmentation angle changes from $\phi = 0$ to $\phi = -\pi/2$ all of the loads remain supported as the same augmentation angle must apply to all loads at a given frequency. There are two simple methods of

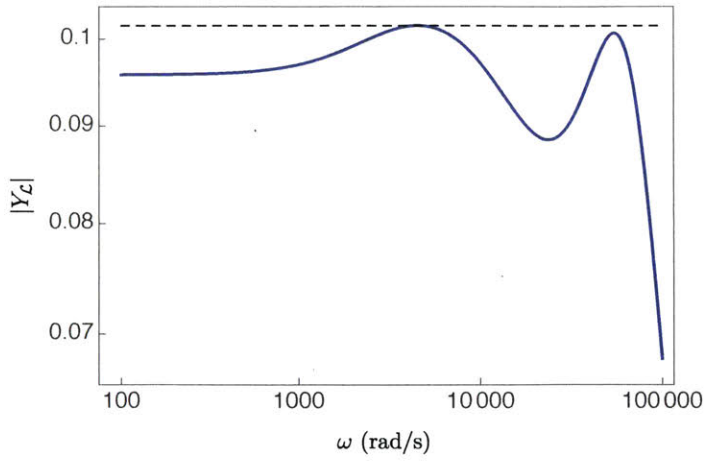

Figure 4-5: Magnitude of the load admittance transfer function bounded from above by $Y_{\max} \approx 0.1016$

applying this constraint. First, in systems with set structure, the smallest Ω_k^L dictates the minimum capacitance required at each load. Conversely, in systems where the filter and stabilizing capacitor have been predetermined, the network structure can be deduced by selecting a line resistance that ensures that each load can be supported by the line to a frequency greater than the largest Ω_k^C.

The bound on the load admittance can easily be found. For an idealized constant power load, the incremental admittance is simply $Y(\omega) = -P/V^2$ where P and V are the equilibrium power consumption and voltage across the load. The load admittance is independent of frequency and therefore the bound on admittance is simply it's magnitude, i.e. $Y_k^{\max} = V^2/P$. Substituting this expression into equation (4.19) or (4.20) allows for necessary (in the framework of the Augmented Power Dissipation method) stability conditions for the network parameters to be calculated. For more complicated load models or for experimental use, an upper bound on the absolute value of admittance can be evaluated numerically. For example, the magnitude of the admittance transfer function for a simple buck converter is given in Figure 4-5 and the upper bound of the admittance magnitude can be discerned graphically. This upper bound is frequency independent; however, unlike with the CPL, the network is only required to be sufficiently conductive for frequencies below the crossover frequency Ω_c.

	Parameter	Description	Value
Converter	V	Input Voltage	28V
	R	Load Resistance	3 Ω
	C	Capacitance	500 μF
	L	Inductance	50 μH
	D	Duty Cycle	0.536
Controller	$G_{c\infty}$	Midband Gain	3.7
	ω_L	Lead Zero	500 Hz
	ω_z	Trailing Zero	1700 Hz
	ω_p	Pole	14.5 kHz
	H	Sensor Gain	$\frac{1}{3}$
	V_m	Voltage of PWM	4

Table 4.2: Converter and Control Parameters

4.2 Numerical Simulation

For simplicity, the following numerical simulations will consider the same power electronic load interfaced with different network configurations. We model the load as a constant resistance load interfaced with the network through a traditional buck converter. The converter output voltage is maintained through the addition of a simple lead-lag controller of the form

$$G_c(s) = G_{c\infty}\frac{\left(1+\frac{\omega_L}{s}\right)\left(1+\frac{s}{\omega_z}\right)}{\left(1+\frac{s}{\omega_p}\right)}. \tag{4.21}$$

The converter and controller parameters have been drawn from [11] and are defined in Table 4.2. The crossover frequency, Ω_c, is 4.8kHz or 30160 rad/s. The admittance magnitude for this load bounded from above such that $Y^{\max} \approx 0.1016$, which can be deduced from the model.

In this section we present three examples of the application of the *Augmented Dissipation* criterion. The first and second examples rely on path decomposition at all frequencies as the capacitors are not necessarily located on the same bus as the loads they support. One example demonstrates how the criterion allows for flexible network structures while the other shows how, even with traditional network structures, a network can support more loading through the use of nontraditional

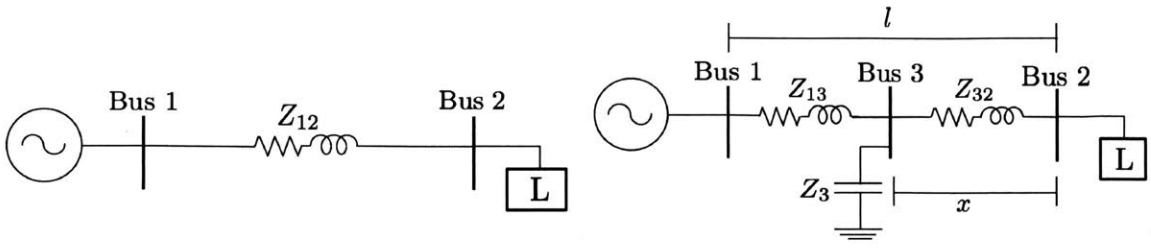

(a) Original System (b) System with addition of stabilizing capacitor

Figure 4-6: 2 bus system for capacitor placement

path decomposition. The final example utilizes the upper bound on dissipation and shows the ease with which stabilizing constraints can be deduced in this formulation.

4.2.1 Path Decomposition: Capacitor Placement

These path decomposition method does not assume nor require a capacitor to be present at each load bus but rather provide guidance on the placement of capacitors that can support a variety of loads. To illustrate this, we will consider a simple two bus system, given in Figure 4-6, comprised of a constant voltage source and a buck converter load connected through a line, with converter parameters and control settings remain the same as in the previous example. While this system is simple, the methodology utilized in this analysis can easily be replicated for more complex network topologies.

In the absence of a capacitor in the network, the system stability can be certified by the line connecting buses 1 and 2 for $\omega \leq \Omega^L = 337.17$ Hz, as derived in Equation (4.19). The addition of a capacitor must therefore certify the stability of the system for $\Omega^L < \omega < \Omega_c$ via a path to the ground. The simplest case is the placement of the capacitor at bus 2 such that the path to certify stability consists only of the added capacitor. In this case, the there are no inductive elements to diminish the Augmented Conductance at high frequencies. The Augmented Conduction of a capacitive element is given by $G = -\omega C \sin(\phi(\omega))$. Given the time-constant τ_L of resistive inductive elements, the largest rotation for which all elements remain passive is given by $\phi(\omega) = -\arctan((\omega\tau_L)^{-1})$. At the maximum negative augmentation angle,

the conductance of the capacitive path is given by

$$G_{\Pi_k} = \frac{\omega C_k}{\sqrt{1 + (\omega \tau_L)^2}} \tag{4.22}$$

Therefore, a capacitor can certify stability for frequencies $|\omega| > \Omega_k^C$ with Ω_k^C given by

$$\Omega_k^C = \frac{Y_k^{\max}}{\sqrt{C_k^2 - (Y_k^{\max} \tau_L)^2}} \tag{4.23}$$

Thus, the required capacitance is found by imposing the requirement that the line and capacitor frequency bands must overlap resulting in the constraint that $C > 96\mu F$.

However, the use of path decomposition and the explicit consideration of the load crossover frequency allows for the certification of the stability of networks where the loads and capacitors are not co-located. In this case, the path to ground consists of the line connecting buses 2 and 3 and has a total impedance of $Z_\Pi = R_{23} + j(\omega L_{23} - (\omega C)^{-1})$. The corresponding augmented conductance is

$$G_\Pi(\phi(\omega)) = \frac{R\cos(\phi(\omega)) + \left(\omega L - \frac{1}{\omega C}\right)\sin(\phi(\omega))}{|Z_\Pi|^2}. \tag{4.24}$$

To adhere to the requirement that all elements remain passive, the rotation $\phi(\omega)$ is limited to the range $-\arctan(\omega\tau) \geq \phi \leq 0$, since both cases contain only resistive-inductive elements or capacitive elements. Since this path contains inductive and capacitive elements the rotation ϕ that results in the largest Augmented Conductance changes with ω. At low frequencies, the maximum Augmented Conductance is limited by the line. At high frequencies, the optimal Augmented Conductance would be achieved by a positive ϕ. However, this rotation would cause the contribution from the capacitive elements to become negative and thus is not allowed. Therefore, at high frequencies, the largest allowable Augmented Conductance is found with $\phi = 0$.

Figure 4-7 shows the Augmented Conductance of the path through the full line to the source and the path through a segment of the line and the capacitor to the ground with $x = 0.1$km and $C = 140\mu$F. For all frequencies below the crossover frequency, Ω_c, one of these paths has an Augmented Conductance that exceeds the maximum load

Parameter	Description	Value
l	Line Length between Buses 1 and 2	5 km
r	Resistance per km	0.2 Ω/km
τ	Line Time Constant	1 ms

Table 4.3: Capacitor Placement Network Parameters

admittance magnitude and therefore stability is guaranteed. It is of note that there are no paths that certify system stability at frequencies slightly above Ω_C, however, since the system is passive in this region there is no requirement for stabilization. As in the previous example, this is an example decomposition and is not intended to present the minimum acceptable capacitance.

The capacitor could be placed away from the load without compromising stability because a buck converter becomes passive at large frequencies mitigating the concern surrounding decaying conductance of the path to the capacitor due to the inductive elements in the lines. For loads that do not become passive at any frequency, such as ideal constant power loads, this methodology dictates that a capacitor must be placed directly at the load bus. This placement ensures that the Augmented Conductance does not tend toward 0 at very high frequencies due to passing through the inductive element. By considering the magnitude of the transfer function and the crossover frequency of a buck converter rather than approximating it with a constant power load, a greater variety of network topologies can be certified to be stable.

4.2.2 Path Decomposition: Multi-Microgrid

We now consider the interconnection of two microgrids, each represented by a voltage source connected to an aggregated load by an inductive-resitive line as given in Figure 4-8. L_{I} and L_{II} are again power electronic loads whose parameters are given in Table 4.2. The network parameters are given in Table 4.4.

According to discussion in the previous section, stability certification at at low frequencies is done by choosing paths from loads to sources passing through inductive-resistive lines. This can only be done without any augmentation, i.e. $\phi(\omega) = 0$ in order to prevent capacitive elements from injecting the Augmented Power. At

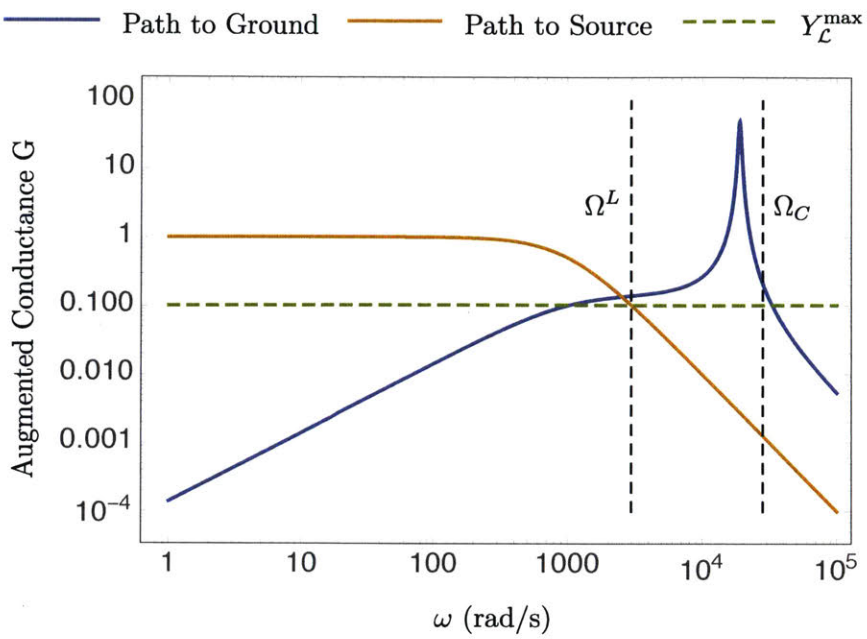

Figure 4-7: Augmented Conductance G of paths to the source and ground given a capacitor placed at $x/l = 1/50$.

high frequencies, the paths should go through capacitive elements to the ground and rotation by a negative non-zero angle is required for capacitors to provide positive Augmented Conductance $G(\omega, \phi(\omega))$. However, the rotation angle is now limited by the condition that the Augmented Conductance of inductive-resisteve elements be at least non-negative which is possible if $|\phi(\omega)| < \arctan((\omega\tau_{max})^{-1})$, where τ_{max} is the maximum value of L/r for lines in the network. In our case we assume all the lines to have the same $\tau = 1ms$ which plays the role of τ_{max}.

In the configuration shown by Fig. 4-8, L_{I} is supported at low frequencies by a path to the source at bus 1 and at high frequencies by the capacitor at bus 2 while L_{II} is supported at low frequencies by a path to the source at bus 4 and at high frequencies by the capacitor at bus 3. These paths do not overlap and thus no elements must be split. The Augmented Conductances of the paths supporting each load are given in Figure 4-9. In order to provide the continuous support, these frequency bands should overlap for both of the loads. The overall Augmented Conductance supporting both loads of example from Fig. 4-8 at all the frequency range is shown by the bolded sections of the path Augmented Conductances. A non-zero ϕ was chosen to begin at

ω = 9000 (rad/s) which is below the crossover frequency of each load but above Ω^C for each load, the minimum frequency at which the capacitors can certify stability.

In the configuration shown by Fig. 4-8, the line connecting buses 2 and 3 is not utilized to support any of the loads. By utilizing this line and it is possible to support additional load. An additional load on bus 2 could be supported through alternate paths such as to the source on bus 4 through the lines connecting buses 2 and 4 for low frequencies and to the capacitor at bus 3 via the line connecting buses 2 and 3 at high frequencies. However, utilizing these paths requires a decomposition of Z_{34} at low frequencies, as in Figure 4-10a, and Z_3 at high frequencies, as in Figure 4-10b. In this decomposition, the superscripts refer to the load being supported by the corresponding network element.

Figure 4-11 gives the results of an example decomposition of the system and demonstrates how an additional load at bus 2 can be supported while still providing enough Augmented Conduction for original loads. It is important to note that this decomposition is not unique and the maximum additional load, that can be supported is related specifically to the decomposition chosen. Further, the rotation $\phi(\omega)$ that we use to provide support at high frequencies is altered from the maximum allowed because the path containing both the line 23 and the capacitor 3 requires an augmentation different than what gives the maximum for the capacitor, since then the line Augmented Conductance will be zero and an overall path will provide no support. In addition, the rotation chosen must still guarantee that the original loads are still supported. The contribution of the line 23 to the high-frequency path for load 3 can be seen on Fig. 4-11 where the Augmented Conductance for this path starts to decrease with frequency after certain point due to decreasing line conductance.

The maximum magnitude of load 3 that could be supported is based upon the minimum value of the Augmented Conductance available on it's paths over the frequency range $\omega < \Omega_c$. In Figure 4-11, the crossover frequency is assumed to be the same for all the loads in the systems and the maximum magnitude that could be supported is $Y_{LIII}^{\max} \approx 0.011$ and the additional decomposition allows for a 10% increase in loading on bus 2.

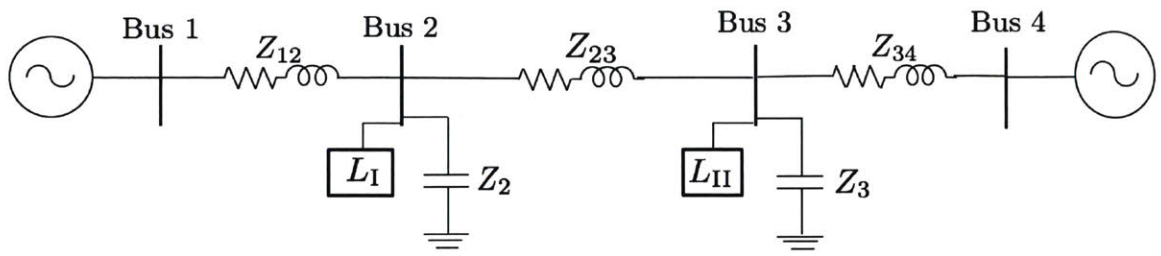

Figure 4-8: 4 bus system representing the interconnection of two microgrids, each comprised of a source and a load.

Parameter	Description	Value
l_{12}	Line Length between Buses 1 and 2	0.5 km
C_2	Capacitance at Bus 2	408.5 μF
l_{23}	Line Length between Buses 2 and 3	1.0 km
C_3	Capacitance at Bus 3	713.1 μF
l_{34}	Line Length between Buses 3 and 4	0.25 km
r	Line Resistance	0.2 Ω/km
τ	Time Constant of All Lines	1 ms

Table 4.4: Multi-Microgrid Network Parameters

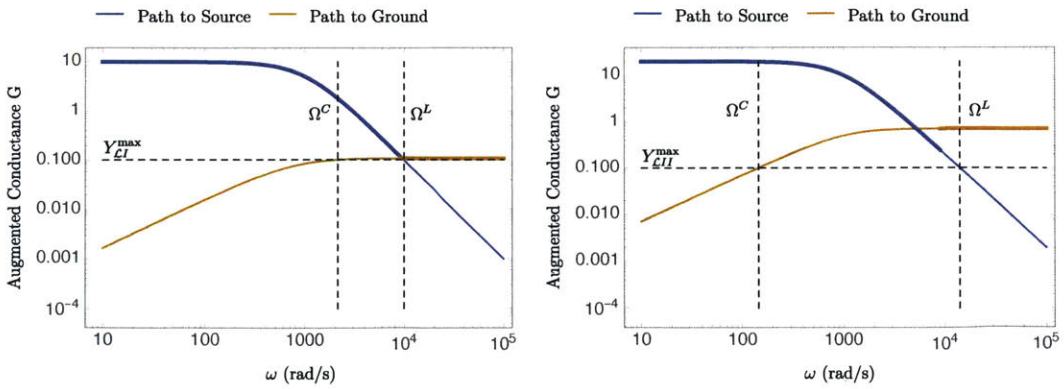

(a) L_{I} (b) L_{II}

Figure 4-9: Augmented conductance of paths supporting L_{I} and L_{II} before the addition of L_{III}. The bolded sections represent the overall augmented conductance based on a consistent admissible $\phi(\omega)$.

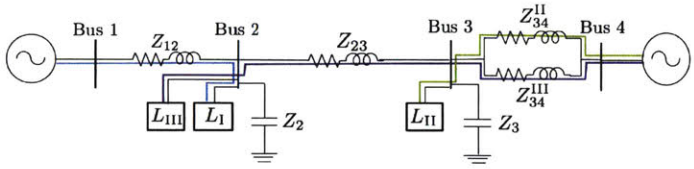

(a) Low Frequency

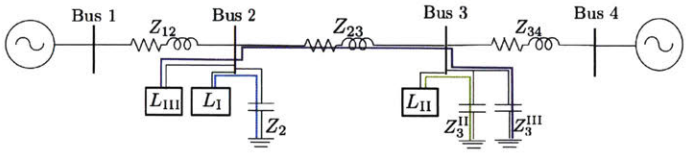

(b) High Frequency

Figure 4-10: High and low frequency path decomposition of the 4 bus multi microgrid system shown in Figure 4-8

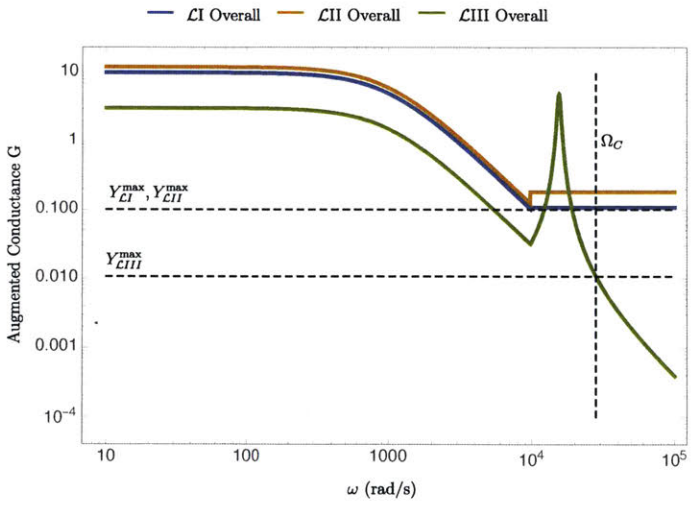

Figure 4-11: Augmented conductance G of paths supporting L_{I}, L_{II} and L_{III}

Parameter	Description	Value
l_{12}	Line Length between Buses 1 and 2	0.5 km
l_{23}	Line Length between Buses 2 and 3	2.5 km
r	Line Resistance	0.2 Ω/km
L_2, L_3	Filter Inductance	330 μH
R_2, R_3	Filter Resistance	2 $\mu\Omega$
τ	Time Constant of All Lines	1 ms

Table 4.5: 3 Bus Network Parameters

4.2.3 Dissipation Upper Bound: 3 Bus System

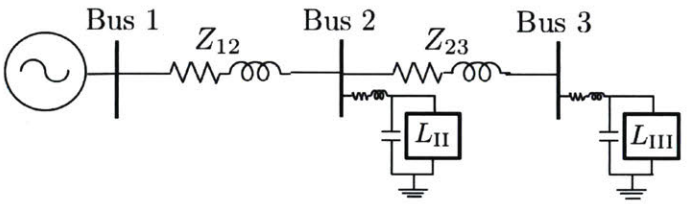

(a) Initial 3 bus set up

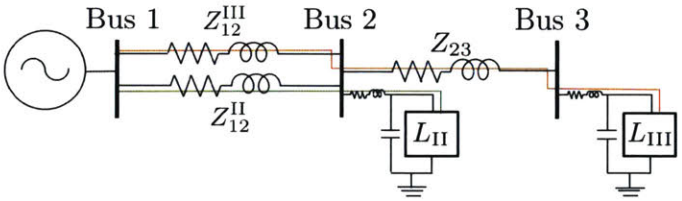

(b) Decomposition into Low Frequency Paths

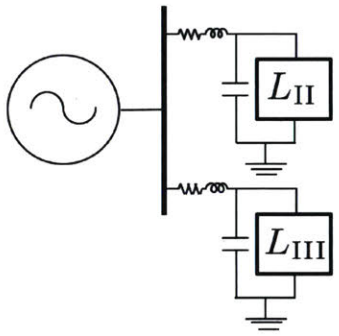

(c) Collapse of network to "star" configuration

Figure 4-12: 3 Bus System

The previous two simulations required a path decomposition at high frequencies due to the stabilizing capacitor and the load not being co-located. As previously established, the reduction of a complex network to a "star" configuration on a common bus allows for a much more reasonable estimate of the bound on the load admittance when there is a capacitor placed at each load. This example will examine such a case by considering a simple three bus network, as shown in Figure 4-12a, with two identical power electronic loads, whose parameters are again given in Table 4.2. The corresponding system parameters are given in Table 4.5.

The network can be reduced into worst case configurations as follows. At low

frequencies, just as with the previous examples, this network can easily be decomposed into paths as given in Figure 4-12b. However, at high frequencies, the loads are connected onto a single infinite bus, as in Figure 4-12c.

Figure 4-13a gives the frequency at which the capacitor can support a load, Ω^C as a function of the capacitance. One curve can be used for the two loads because they have identical filter resistance and inductance. Of note is that $\Omega^L_{\mathcal{L}_{\text{III}}} < \Omega^L_{\mathcal{L}_{\text{II}}}$ because the path from the load at bus 3 has a smaller overall admittance. For both loads to be supported, not only do the frequency bands for which the line and capacitor support each individual load need to overlap, but also there must be a a single frequency frequency band for which all loads can be supported by either augmentation. This overlap ensures that when the system transitions from no augmentation to augmentation by $-\pi/2$ all loads remain supported.

Based on the upper bound on dissipation given in Equation (3.23), a capacitance of 544 μF is required for the frequency bands to meet for L_{III}, namely for $\Omega^L_{\mathcal{L}_{\text{III}}} = \Omega^C_{\mathcal{L}_{\text{III}}}$. The focus is L_{III} because it is the limiting case as the frequency for which the load can be supported through the line is the smallest. Therefore for all frequency bands to overlap any capacitance must be greater than 544 μF as highlighted in Figure 4-13a. To enhance robustness, a capacitance of 576.3 μF was chosen at bus 2 and 652.6μF at bus 3. Figure 4-13b gives the resulting augmented conductances for paths with no augmentation and with augmentation by $-\pi/2$. The bold lines show the conductance as a function of frequency with the transition from no augmentation to an augmentation of $-\pi/2$ at 2382 rad/s.

4.3 Conclusion

This section presents a number of simple examples to understand the implementation of the Augmented Power Dissipation stability certificates. A simple two bus system is presented to provide an understanding as to the effects of different augmentations in a network with resistive-inductive lines, parallel load capacitors and arbitrary loads. Further, we explicitly show that the criterion we derive adhere to the traditional

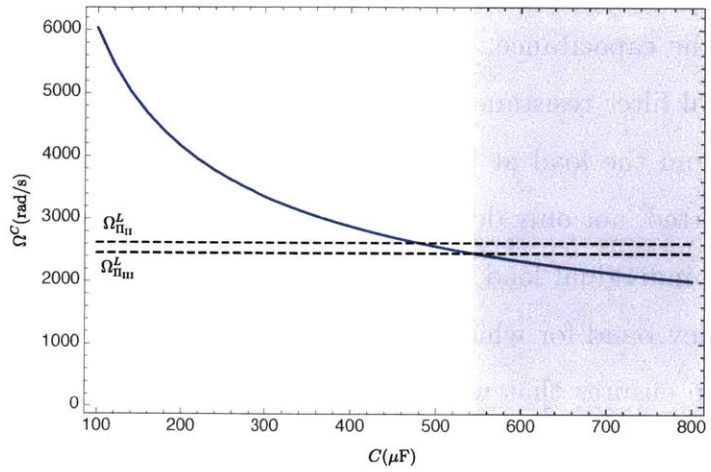

(a) Capacitance required for frequency band overlap of both loads

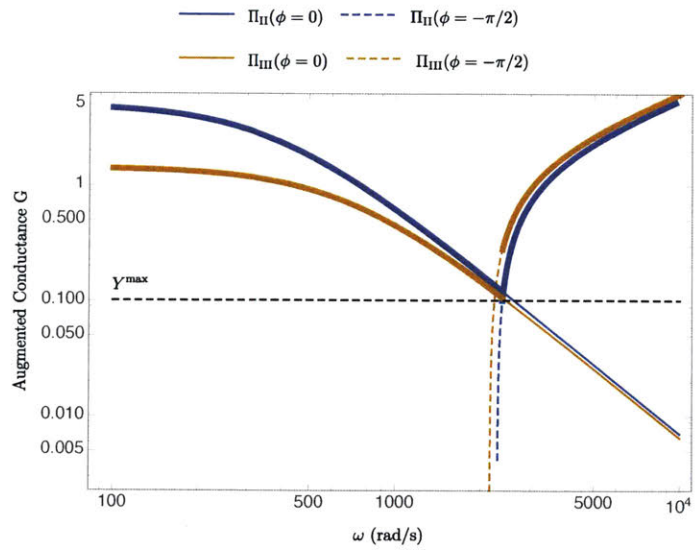

(b) Augmented conductance for L_{II} and L_{III}

Figure 4-13: 3 Bus capacitance required for frequency overlap and the resulting augmented conductances G

Middlebrook criterion across the frequency spectrum. This adherence is critical because it demonstrates that comparable stability constraints can be developed with the network structure explicitly in mind.

The examples provided in this section show the value of the network-aware characteristics of Augmented Power Dissipation stability certificates which differentiate if from the canonical Middlebrook criterion. The examples provided which utilize the network decomposition formulation of the certificates demonstrate how it can easily be used to design network topologies and input filters or to support additional loading via elements located in different parts of the network. In contrast, the example in which the upper bound on dissipation was utilized at high frequencies demonstrated the easy in determining adequate filter capacitances based on the worst case path to a source.

Beyond showing the direct application of these stability criterion to physical systems, these examples also serve to highlight when the differing formulations can be valuable. The network decomposition formulation allows for a greater variety of topologies, most notably separating a stabilizing capacitor from a load. However, at high frequencies, a network decomposition does not take advantage of much of the dissipation of the capacitive elements. In contrast, the method of bounding the dissipation allows for a much simpler system analysis at the cost of prescribing the constraints of a "star-shaped" network and parallel load capacitors. It is of note that there is always some residual shunt capacitance at each load so constraining the system in that way is not inappropriate.

Chapter 5

Concluding Remarks

5.1 Conclusion and Contribution

Microgrids have the potential to be a viable off-grid solution. Electricity access has a significant impact on the developing world and has been linked to increased education, employment and quality of life. As the cost of microgrids decreases, their implementation becomes constrained by stability concerns. This thesis has focused on identifying two specific instabilities that could compromise microgrid performance and developing simple certificates that guarantee the stability of a network. The ultimate goal of this work is to reduce the technical overhead in the network design and therefore allow for the simple and quick deployment of microgrids.

The approaches presented here are unique in that they strive to create simple rules to govern a entire system or local bus that can guarantee stability in the presence of high uncertainty typical for the developing world. These constraints remove a dependence on specific knowledge of the loading by simply requiring a bound on maximum power consumption or admittance magnitude. Further, the structure of these constraints will allow for simple incorporation into optimal dispatch or reconfiguration problems.

The constraints developed were based on the characterization of so-called worst-case configurations or situations. These configurations are powerful in that they allow for a meaningful reduction of complex networks to simple systems that can be

analyzed easily. First, it was shown that the worst case configuration for an arbitrary network was a two bus system with all generation on one bus and all loading on another. We also empirically characterized the worst case load switching event that dictated the required capacitance as the addition of the largest allowable load at a node that brought the full system loading to its maximum Second, the network-aware small signal analysis presented in Chapters 3 and 4 showed that at low frequencies a network can be reduced to a system with a generation source and load connected solely by a line and that at high frequencies the network can be collapsed into a star configuration of loads at a single infinite bus. This methodology is powerful in the insight it allows into complex systems.

The two instabilities studied were the load switching instability in an arbitrary network with constant power loads and the small-signal instability in a network with arbitrary loads. The study of the load switching instability considered an arbitrary network and utilized Brayton Moser Potential theory and Lyapunov analysis for non-linear stability. Through bounding the voltages on all buses at a stable and unstable equilibria, assigning a minimum voltage at equilibrium and a minimum voltage during transients, the capacitance required for the network to remain stable due to a variation in power at a given bus was determined. By optimizing over the domain of all possible variations, it was possible to determine the lower bound on capacitance required to allow for the successful addition or removal of a load from the network. We then identified a critical point above which the capacitance increases superlinearly, highlighting a trade-off between loading and cost associated with the capacitance. Further, our work indicates the maximum power any load can consume based on the desired minimum node voltage. This is an important design limitation to consider when balancing load utility and load voltage sensitivity.

The small signal stability of DC networks is a problem that has been studied extensively. Our work strove to build upon this work by taking into account network dynamics and structure. A certificate was developed based on the positivity of the Augmented Power Dissipation. The first approach based upon this certificate utilized a decomposition of the network into paths starting at a load and ending at the

source or ground. It was shown that as long as these paths had an Augmented Conductance greater than the maximum load magnitude, the load would remain stable. The second approach was based on the the development of an upper bound on the network dissipation. This approach removed the augmentation restrictions at high frequencies and allowed for greater support of the load in that regime.

5.2 Future Directions

The future directions of this research can be placed into two distinct categories: the continued study of specific DC microgrid instabilities and the utilization of the constraints developed in relevant optimization problems.

The comprehensive review presented in [17] emphasized the importance of studying transient stability in microgrids and quantifying the region of attraction. Chapter 2 began to address transient stability concerns in microgrids by presenting a comprehensive study of the load switching instability in microgrids where individual loads can account for large fractions of the total loading. This nonlinear transient stability analysis in was carried out in the time domain through the use of Lyapunov methods. However, much of the traditional work on stability, including the small signal stability work presented in Chapters 3 and 4, takes place in the frequency domain. The ability to join the small signal and transient stability assessments would be a powerful tool and useful for extending nonlinear analysis to uncertain loads.

Because of the unique approach taken in this thesis to characterize worst-case scenarios or configuration, a set of constraints that rely on minimal information about the load or network have been developed that can easily lend themselves to optimization problems that arise within these grids. These problems include optimal reconfiguration and optimal dispatch algorithms. By considering stability explicitly through the constraints of the problem, the physics is coupled with the network analysis to ensure a stable outcome. Further, the constraints developed here were based on limited information about either the network or the load, assuming a perfect constant voltage source model. The expansion of these constraints to include more general

generation and storage models could be meaningful especially in conjunction with optimal dispatch algorithms.

Bibliography

[1] S. Anand and B. G. Fernandes. Reduced-order model and stability analysis of low-voltage dc microgrid. *Industrial Electronics, IEEE Transactions on*, 60(11):5040 – 5049, November 2013.

[2] Karl Johan Astrom and Richard M. Murray. *Feedback Systems: An Introduction for Scientists and Engineers*. Princeton University Press, Princeton, NJ, USA, 2008.

[3] World Bank. *State of electricity access report 2017 (Vol. 2) : full report (English)*. World Bank Group, Washington, D.C., 2017. http://documents.worldbank.org/curated/en/364571494517675149/full-report.

[4] N. Barabanov, R. Ortega, R. Grino, and B. Polyak. On Existence and Stability of Equilibria of Linear Time-Invariant Systems With Constant Power Loads. *IEEE Transactions on Circuits and Systems I: Regular Papers*, 63(1):114–121, 2016.

[5] Julia A Belk, Wardah Inam, David J Perreault, and Konstantin Turitsyn. Stability and control of ad hoc dc microgrids. In *Decision and Control (CDC), 2016 IEEE 55th Conference on*, pages 3271–3278. IEEE, 2016.

[6] S. Bolognani and S. Zampieri. On the Existence and Linear Approximation of the Power Flow Solution in Power Distribution Networks. *IEEE Transactions on Power Systems*, (99):1–10, 2015.

[7] R. Brayton and J. Moser. Some Results on the Stability of Nonlinear Networks Containing Negative Resistances. *IEEE Transactions on Circuit Theory*, 11(1):165–167, 1964.

[8] G. Cezar, R. Rajagopal, and B. Zhang. Stability of interconnected DC converters. In *2015 54th IEEE Conference on Decision and Control (CDC*, pages 9–14. IEEE, 2015.

[9] C. De Persis, E.R.A. Weitenberg, and F. Dörfler. A power consensus algorithm for dc microgrids. In *IFAC World Congress*, November 2017. To appear.

[10] Claudio De Persis, Erik RA Weitenberg, and Florian Dörfler. A power consensus algorithm for dc microgrids. *Automatica*, 89:364–375, 2018.

[11] Robert W Erickson and Dragan Maksimovic. *Fundamentals of power electronics.* Springer Science & Business Media, 2007.

[12] IEA. *World Energy Outlook 2017.* International Energy Agency, 2017.

[13] W. Inam, D. Strawser, K.K. Afridi, R.J. Ram, and D.J. Perreault. Architecture and system analysis of microgrids with peer-to-peer electricity sharing to create a marketplace which enables energy access. In *Power Electronics and ECCE Asia (ICPE-ECCE Asia), 2015 9th International Conference on*, pages 464–469, June 2015.

[14] Wardah Inam. *Adaptable Power Conversion for Grid and Microgrid Applications.* PhD thesis, Massachusetts Institute of Technology, Massachusetts, Cambridge, MA, 2016.

[15] D. Jeltsema and J. Scherpen. Multidomain modeling of nonlinear networks and systems. *IEEE Control Systems Magazine*, 29(4):28–59, 2009.

[16] J. J. Justo, F. Mwasilu, J. Lee, and J. W. Jung. Ac-microgrids versus dc-microgrids with distributed energy resources: A review. *Renewable and Sustainable Energy Reviews*, 24:387–405, 2013.

[17] M. Kabalan, P. Singh, and D. Niebur. Large signal lyapunov-based stability studies in microgrids: A review. *IEEE Transactions on Smart Grid*, 8(5):2287–2295, Sept 2017.

[18] Hannes Kirchoff. Interview, October 2017. CTO SolShare.

[19] Anshuman Lath. Interview, January 2017. Gram Oorja Site Visit.

[20] R.D. Middlebrook. Input filter considerations in design and application of switching regulators. *IEEE IAS Annual Meeting*, 1976.

[21] United Nations. *The Millennium Development Goals Report.* United Nations, 2015.

[22] Antonino Riccobono and Enrico Santi. Comprehensive review of stability criteria for dc distribution systems. In *Energy Conversion Congress and Exposition (ECCE), 2012 IEEE*, pages 3917–3925. IEEE, 2012.

[23] S. Rivera, A. M. Farid, and K. Youcef-Toumi. A multi-agent system transient stability platform for resilient self-healing operation of multiple microgrids. In *ISGT 2014*, pages 1–5, Feb 2014.

[24] S. Sanchez, R. Ortega, G. Bergna, M. Molinas, and R. Grino. Conditions for existence of equilibrium points of systems with constant power loads. In *2013 IEEE 52nd Annual Conference on Decision and Control (CDC)*, pages 3641–3646. IEEE, 2013.

[25] Pannala Sanjeev, Narayana Prasad Padhy, and Pramod Agarwal. Dc grid initiative in india. *IFAC-PapersOnLine*, 48(30):114 – 119, 2015. 9th IFAC Symposium on Control of Power and Energy Systems CPES 2015.

[26] J. W. Simpson-Porco, F. Dörfler, and F. Bullo. On Resistive Networks of Constant-Power Devices. *IEEE Transactions on Circuits and Systems II: Express Briefs*, 62(8):811–815, 2015.

[27] John W Simpson-Porco, Florian Dörfler, and Francesco Bullo. Voltage collapse in complex power grids. *Nature communications*, 7, 2016.

[28] Brenda Boardman John Kimani Stephen Karekezi, Susan McDade. Energy, poverty and development. In *Global Energy Assessment - Toward a Sustainable Future*, chapter 2, pages 151–190. Cambridge University Press, Cambridge, UK and New York, NY, USA and the International Institute for Applied Systems Analysis, Laxenburg, Austria, 2012.

[29] J. Zhao and F. Dörfler. Distributed control and optimization in DC microgrids. *Automatica*, 61:18–26, November 2015.